Comput Geosci (2014) 18:711–728
DOI 10.1007/s10596-014-9418-y

ORIGINAL PAPER

On classical iterative subdomain methods for the Stokes–Darcy problem

Alfonso Caiazzo · Volker John · Ulrich Wilbrandt

Received: 18 December 2013 / Accepted: 20 March 2014 / Published online: 22 April 2014

Abstract Within classical iterative subdomain methods, the problems in the subdomains are solved alternately by only using data on the interface provided from the other subdomains. Methods of this type for the Stokes–Darcy problem that use Robin boundary conditions on the interface are reviewed. Their common underlying structure and their main differences are identified. In particular, it is clarified that there are different updating strategies for the interface conditions. For small values of fluid viscosity and hydraulic permeability, which are relevant in applications from geosciences, it is shown in numerical studies that only one of these updating strategies leads to an efficient numerical method, if it is used with appropriate parameters in the Robin conditions.

Keywords Stokes–Darcy problem · Classical iterative subdomain methods · Robin boundary conditions · Finite element methods · Continuous and discontinuous updating strategy · Applications from geosciences

1 Introduction

Consider a bounded domain $\Omega \subset \mathbb{R}^d$, $d \in \{2, 3\}$, and a decomposition $\Omega = \Omega_\mathrm{f} \cup \Gamma_\mathrm{I} \cup \Omega_\mathrm{p}$ into two disjoint subdomains Ω_f and Ω_p, denoting a free flow domain and a porous medium, respectively, and possessing a common interface Γ_I, i.e., $\Omega_\mathrm{f} \cap \Omega_\mathrm{p} = \emptyset$ and $\overline{\Omega_\mathrm{f}} \cap \overline{\Omega_\mathrm{p}} = \Gamma_\mathrm{I}$. Assuming a moderate flow velocity in the free flow domain, the fluid dynamics in Ω_f can be modeled with the incompressible Stokes equations for the velocity $\mathbf{u}_\mathrm{f} : \Omega_\mathrm{f} \to \mathbb{R}^d$ [m/s] and the pressure $P_\mathrm{f} : \Omega_\mathrm{f} \to \mathbb{R}$ [Pa]

$$\nabla \cdot \mathbb{T}\left(\mathbf{u}_\mathrm{f}, \frac{P_\mathrm{f}}{\rho}\right) = \mathbf{f}_\mathrm{f} \text{ in } \Omega_\mathrm{f}, \tag{1}$$

$$\nabla \cdot \mathbf{u}_\mathrm{f} = 0 \text{ in } \Omega_\mathrm{f}. \tag{2}$$

In Eq. (1), ρ [kg/m^3] represents the fluid density, and the fluid stress tensor $\mathbb{T}(\mathbf{u}_\mathrm{f}, p_\mathrm{f})$ [m^2/s^2] is defined by

$$\mathbb{T}(\mathbf{u}_\mathrm{f}, p_\mathrm{f}) : \Omega_\mathrm{f} \to \mathbb{R}^{d\times d}, \quad \mathbb{T} = 2\nu\mathbb{D}(\mathbf{u}_\mathrm{f}) - p_\mathrm{f}\mathbb{I},$$

where $\mathbb{D}(\mathbf{u}_\mathrm{f}) = (\nabla\mathbf{u} + \nabla\mathbf{u}^T)/2 : \Omega_\mathrm{f} \to \mathbb{R}^{d\times d}$ [1/s] is the velocity deformation tensor, $p_\mathrm{f} = P_\mathrm{f}/\rho$ [m^2/s^2], and $\nu : \Omega_\mathrm{f} \to \mathbb{R}$ [m^2/s] denotes the kinematic viscosity of the fluid. Outer forces acting on the free flow are modeled by $\mathbf{f}_\mathrm{f} : \Omega_\mathrm{f} \to \mathbb{R}^d$ [m/s^2].

The dynamics in the porous medium is described by the Darcy law:

$$\mathbb{K}\nabla\varphi_\mathrm{p} + \mathbf{u}_\mathrm{p} = \mathbf{0} \text{ in } \Omega_\mathrm{p}, \tag{3}$$

$$\nabla \cdot \mathbf{u}_\mathrm{p} = f_\mathrm{p} \text{ in } \Omega_\mathrm{p}, \tag{4}$$

in terms of $\varphi_\mathrm{p} : \Omega_\mathrm{p} \to \mathbb{R}$ [m], called Darcy pressure or piezometric head, and of the Darcy velocity $\mathbf{u}_\mathrm{p} : \Omega_\mathrm{p} \to \mathbb{R}^d$ [m/s]. In Eq. (3), $\mathbb{K} : \Omega_\mathrm{p} \to \mathbb{R}^{d\times d}$ [m/s] is the hydraulic conductivity tensor. Generally, it is assumed that $\mathbb{K} = \mathbb{K}^T$, $\mathbb{K} > 0$. Here, only the case $\mathbb{K} = K\mathbb{I}$, $K > 0$, will be

A. Caiazzo · V. John (✉) · U. Wilbrandt
Weierstrass Institute for Applied Analysis and Stochastics (WIAS), Mohrenstr. 39, 10117 Berlin, Germany
e-mail: john@wias-berlin.de

V. John
Department of Mathematics and Computer Science, Free University of Berlin, Arnimallee 6, 14195 Berlin, Germany

considered. In Eq. (4), the function $f_p : \Omega_p \to \mathbb{R}$ [1/s] describes sinks and sources. System (3)–(4) is called the mixed form of the Darcy problem. An alternative formulation is obtained by taking the divergence of Eq. (3) and using (4),

$$-\nabla \cdot (\mathbb{K}\nabla\varphi_p) = f_p \text{ in } \Omega_p, \tag{5}$$

which is called the primal form of the Darcy problem.

The mixed form is often more important for applications, as it recovers the Darcy velocity $\mathbf{u}_p$ directly. However, we will focus on the primal formulation because of its simplicity. For the studied numerical methods, there are still open questions for this formulation.

System (1), (2), and (5) must be completed with appropriate boundary conditions and with proper interface conditions at the Stokes–Darcy interface Γ_I. Denote by $\mathbf{n}_f$ and $\mathbf{n}_p$ the unit outward normal vectors on $\partial\Omega_f$ and $\partial\Omega_p$, respectively, and by $\boldsymbol{\tau}_i$, $i = 1, \ldots, d-1$, pairwise orthogonal unit tangential vectors on the interface Γ_I. Note that $\mathbf{n}_f = -\mathbf{n}_p$ on Γ_I. Two standard coupling conditions on Γ_I model the conservation of mass and the balance of normal stresses

$$\mathbf{u}_f \cdot \mathbf{n}_f = -\mathbb{K}\nabla\varphi_p \cdot \mathbf{n}_f \text{ on } \Gamma_I, \tag{6}$$

$$-\mathbf{n}_f \cdot \mathbb{T}(\mathbf{u}_f, p_f) \cdot \mathbf{n}_f = g\varphi_p \quad \text{on } \Gamma_I, \tag{7}$$

where g [m/s^2] is the gravitational acceleration. A classical third coupling condition is the so-called Beavers–Joseph–Saffman condition [19, 25] (also Beavers–Joseph–Saffman–Jones condition), which is based on experimental findings relating the tangential velocity along the interface to the fluid stresses:

$$\mathbf{u}_f \cdot \boldsymbol{\tau}_i + \alpha \boldsymbol{\tau}_i \cdot \mathbb{T}(\mathbf{u}_f, p_f) \cdot \mathbf{n}_f = 0 \quad \text{on } \Gamma_I, i = 1, \ldots, d-1, \tag{8}$$

where $i = 1, \ldots, d-1$, $\alpha = \alpha_0 \sqrt{(\boldsymbol{\tau}_i \cdot \mathbb{K} \cdot \boldsymbol{\tau}_i)/(\nu g)}$ [s/m], and $\alpha_0 > 0$ is a nondimensional parameter depending on properties of the porous medium. A simplification is based on the observation that both terms on the left-hand side of Eq. (8) are small, leading to

$$\mathbf{u}_f \cdot \boldsymbol{\tau}_i = 0 \quad \text{on } \Gamma_I, i = 1, \ldots, d-1. \tag{9}$$

The coupled problem defined by Eqs. (1), (2), and (5) with the conditions (6), (7), and (8) (or (9)) has been studied extensively in the literature both theoretically; see, among others, [1, 6, 17, 21], and numerically, e.g., in [5, 9, 12–14, 16, 20, 24, 28].

Numerical methods for solving the coupled problem might be divided into two main classes. Direct, monolithic, or single-domain methods aim at solving the coupled system in a single step. Proposals of finite element-based approaches in this class can be found, e.g., in [2–4, 16, 22, 26, 27]. As an alternative, decoupled, domain-decomposition, or multidomain approaches solve the coupled problem with a subdomain iterative procedure based, at each iteration, on the solution of the Stokes and Darcy problem separately. On the one hand, an iterative method requires multiple solutions of the subproblems. On the other hand, these techniques allow to use specialized solvers for Stokes and Darcy problems and to tailor the algorithms according to their mathematical and physical properties, which might result in efficient procedures. Furthermore, iterative approaches are generally preferred if efficient solvers for the subproblems are available.

Our interest in the Stokes–Darcy problem comes from the numerical simulation of the fluid dynamics in water basins and river beds. These problems are characterized by complex geometries, and their discretization might lead to large systems. For this reason, and also since an efficient code for the simulation of incompressible free flows and scalar elliptic problems is available [18], the use of iterative strategies is our preferred option. The classical approach of iterative subdomain methods consists in solving the equation in one subdomain, provide data on the interface for the other subdomain, do the same for the other subdomain, and repeat this procedure until convergence is achieved. An extension of this strategy consists in embedding the classical approach into a Krylov method for an appropriate interface equation, as it is often done in domain decomposition methods. We think that, because of its simplicity, the classical approach is more likely to be adopted from practitioners in geosciences who are developing their own software. Therefore, we will concentrate in this paper on the classical approach.

Surveying the literature on iterative methods, one finds different strategies concerning the splitting of the interface conditions. This splitting defines the boundary condition on Γ_I for the individual Stokes and Darcy problems. A first approach, called here Neumann–Neumann coupling, consists in solving Neumann problems in both subdomains. It is reported to perform well for large values of viscosity and hydraulic conductivity, $\nu \approx 1$, $K \approx 1$. However, it has been shown in [14] that it converges very slowly on fine meshes for small ν and K, a configuration which is of utmost importance for applications in geosciences, where, e.g., $\nu = 10^{-6}$ [m^2/s] (water) and $K \in [10^{-9}, 10^{-3}]$ [m/s] (clay, sand, gravel) are values of interest.

To overcome these problems, it was first proposed in [14] to use Robin problems rather than Neumann problems. The numerical results in [14], obtained with a classical subdomain iteration, are very promising, showing that the Robin–Robin coupling is robust and efficient in the parameter range that is of interest for geoscientific applications. This coupling introduces two parameters γ_f and γ_p, which specify the linear combination of the essential and natural boundary condition for the Stokes and Darcy problems,

respectively. As shown in [14], these parameters have to be tuned in order to achieve fast convergence of the iterative scheme. After the pioneering work of [14], more variants of Robin–Robin iterative methods have been proposed and analyzed (see, e.g., [5, 6, 9]).

The motivation of our work is the fact that the choice of the two parameters γ_f and γ_p is to some extent unclear. The numerical analysis in [14] suggests that the Robin parameters should satisfy $\gamma_\mathrm{f} > \gamma_\mathrm{p}$, at least for ν, $K \ll 1$. On the other hand, in [9], it is shown that the convergence is fast only for $\gamma_\mathrm{f} \leq \gamma_\mathrm{p}$ at least for $\nu \approx 1$, $K \approx 1$. This puzzling situation is of course unsatisfactory and makes the usage of a Robin–Robin coupling prohibitive in practical applications. In particular, several questions remain to be addressed, concerning the dependence of the numerical parameters on the coefficients of the problem.

In this paper, a unified presentation of the considered algorithms will be given, thereby identifying the common underlying structure and highlighting their differences. It will be clarified that different updating strategies for the Robin conditions on the interface can be applied. One of them, called here continuous Robin–Robin (C-RR), is based on rewriting the Neumann–Neumann formulation as a Robin–Robin formulation, whereas the other one, called discontinuous Robin–Robin (D-RR), directly uses a Robin–Robin formulation of the coupled problem. The algorithms will be assessed for problems whose coefficients are of the magnitude which is relevant for applications from geosciences. It will turn out that only one of the updating strategies leads to efficient methods, if it is used with appropriately chosen parameters in the Robin conditions. A detailed numerical study and some arguments concerning the norm of the iteration matrices provide new insight in the choice of γ_f and γ_p. In particular, it will be shown that the parameters can be chosen such that $\gamma_\mathrm{f}/\gamma_\mathrm{p}$ is considerably larger than proposed so far in the literature.

The paper is organized as follows. Section 2 introduces the variational and the finite element formulations of the coupled problems, while Section 3 focuses on the classical iterative strategies considered in the paper. Computational results are presented in Section 4, and a summary and an outlook are given in Section 5.

2 Weak formulation of the Stokes–Darcy problem

This section introduces the weak formulation of the Stokes–Darcy problem together with different strategies for including the interface conditions.

For an open set $\omega \subset \mathbb{R}^d$, let $H^m(\omega)$ denote the standard Sobolev spaces, and let $L^2(\omega) = H^0(\omega)$. In addition, $(\cdot,\cdot)_\omega$ denotes the $L^2(\omega)$ inner product, and $\langle\cdot,\cdot\rangle_{\Gamma_\mathrm{I}}$ stands for the inner product in $L^2(\Gamma_\mathrm{I})$.

2.1 Weak formulation

It will be assumed, without loss of generality, that the Eqs. (1), (2), and (5) and the interface conditions (6), (7), and (8) (or (9)) are nondimensionalized with unity characteristic scales such that the nondimensional equations have exactly the same form. As usual, the Stokes pressure is defined such that it incorporates the density. For simplicity of presentation, it will not be distinguished between dimensional and nondimensional quantities.

Besides interface conditions on Γ_I, also boundary conditions on the external boundaries $(\partial\Omega_\mathrm{f} \cup \partial\Omega_\mathrm{p}) \setminus \Gamma_I$ have to be specified. In what follows, homogeneous conditions will be considered. However, the presented arguments can be extended also to the nonhomogeneous case. The boundary parts where essential conditions are prescribed are denoted by $\Gamma_{\mathrm{f},e}$ and $\Gamma_{\mathrm{p},e}$, respectively, and it will be assumed that $|\Gamma_{\mathrm{f},e}| > 0$ and $|\Gamma_{\mathrm{p},e}| > 0$.

For the derivation of a weak formulation, the essential boundary conditions are incorporated into the function spaces. Hence, the space for the Stokes velocity is defined by

$$V_\mathrm{f} = \left\{ \mathbf{v} \in \left(H^1(\Omega_\mathrm{f})\right)^d \ : \mathbf{v} = \mathbf{0} \text{ on } \Gamma_{\mathrm{f},e} \right\}.$$

The pressure is sought in $Q_\mathrm{f} = L^2(\Omega_\mathrm{f})$. For the Darcy problem, the space for the piezometric head is given by

$$Q_\mathrm{p} = \left\{ \psi \in H^1(\Omega_\mathrm{p}) \ : \ \psi = 0 \text{ on } \Gamma_{\mathrm{p},e} \right\}.$$

The weak formulations of the Stokes and the Darcy equations are derived in a standard way by multiplying (1), (2), and (5) with appropriate test functions and applying integration by parts. Due to the choice of the boundary conditions, all integrals on $(\partial\Omega_\mathrm{f} \cup \partial\Omega_\mathrm{p}) \setminus \Gamma_I$ vanish. One obtains the following weak form of the Stokes–Darcy problem: Find $(\mathbf{u}_\mathrm{f}, p_\mathrm{f}, \varphi_\mathrm{p}) \in V_\mathrm{f} \times Q_\mathrm{f} \times Q_\mathrm{p}$ such that for all $(\mathbf{v}, q, \psi) \in V_\mathrm{f} \times Q_\mathrm{f} \times Q_\mathrm{p}$

$$\begin{aligned}(\mathbb{T}(\mathbf{u}_\mathrm{f}, p_\mathrm{f}), \mathbb{D}(\mathbf{v}))_{\Omega_\mathrm{f}} + (\nabla\cdot\mathbf{u}_\mathrm{f}, q)_{\Omega_\mathrm{f}} - \langle \mathbb{T}(\mathbf{u}_\mathrm{f}, p_\mathrm{f})\cdot\mathbf{n}_\mathrm{f}, \mathbf{v}\rangle_{\Gamma_\mathrm{I}} \\ = (\mathbf{f}_\mathrm{f}, \mathbf{v})_{\Omega_\mathrm{f}}, \qquad (10)\end{aligned}$$

$$\left(\mathbb{K}\nabla\varphi_\mathrm{p}, \nabla\psi\right)_{\Omega_\mathrm{p}} + \left\langle \mathbb{K}\nabla\varphi_\mathrm{p}\cdot\mathbf{n}_\mathrm{f}, \psi\right\rangle_{\Gamma_\mathrm{I}} = \left(f_\mathrm{p}, \psi\right)_{\Omega_\mathrm{p}}. \qquad (11)$$

The Beavers–Joseph–Saffman condition (8) can be included naturally into the weak formulation (10).

Decomposing the integral over $\Gamma_{\rm I}$ in (10) into normal and tangential components gives

$$a_{\rm f}(\mathbf{u}_{\rm f},\mathbf{v})+b_{\rm f}(\mathbf{v},p_{\rm f})-b_{\rm f}(\mathbf{u}_{\rm f},q)-\langle\mathbf{n}_{\rm f}\cdot\mathbb{T}(\mathbf{u}_{\rm f},p_{\rm f})\cdot\mathbf{n}_{\rm f},\mathbf{v}\cdot\mathbf{n}_{\rm f}\rangle_{\Gamma_{\rm I}} = (\mathbf{f}_{\rm f},\mathbf{v})_{\Omega_{\rm f}}, \tag{12}$$

$$a_{\rm p}(\varphi_{\rm p},\psi)+\langle\mathbb{K}\nabla\varphi_{\rm p}\cdot\mathbf{n}_{\rm f},\psi\rangle_{\Gamma_{\rm I}} = (f_{\rm p},\psi)_{\Omega_{\rm p}}, \tag{13}$$

with $a_{\rm f}: V_{\rm f}\times V_{\rm f}\to\mathbb{R}$, $b_{\rm f}: V_{\rm f}\times Q_{\rm f}\to\mathbb{R}$, and $a_{\rm p}: Q_{\rm p}\times Q_{\rm p}\to\mathbb{R}$ defined by

$$a_{\rm f}(\mathbf{u},\mathbf{v}) = (2\nu\mathbb{D}(\mathbf{u}),\mathbb{D}(\mathbf{v}))_{\Omega_{\rm f}}+\sum_{i=1}^{d-1}\frac{1}{\alpha}\langle\mathbf{u}\cdot\boldsymbol{\tau}_i,\mathbf{v}\cdot\boldsymbol{\tau}_i\rangle_{\Gamma_{\rm I}},$$

$$b_{\rm f}(\mathbf{v},p) = -(\nabla\cdot\mathbf{v},p)_{\Omega_{\rm f}},$$

$$a_{\rm p}(\varphi,\psi) = (\mathbb{K}\nabla\varphi,\nabla\psi)_{\Omega_{\rm p}}.$$

For the simplified interface condition (9), one obtains equations of the same form as (12)–(13) with

$$a_{\rm f}(\mathbf{u},\mathbf{v}) = (2\nu\mathbb{D}(\mathbf{u}),\mathbb{D}(\mathbf{v}))_{\Omega_{\rm f}}.$$

2.2 Neumann–Neumann coupled formulation

For completeness of presentation and for highlighting the differences to the Robin–Robin approach, first the Neumann–Neumann coupled formulation is reviewed. Inserting the interface conditions (7) and (6) into (12)–(13) yields the Stokes–Darcy weak formulation

$$a_{\rm f}(\mathbf{u}_{\rm f},\mathbf{v})+b_{\rm f}(\mathbf{v},p_{\rm f})-b_{\rm f}(\mathbf{u}_{\rm f},q)+\langle g\varphi_{\rm p},\mathbf{v}\cdot\mathbf{n}_{\rm f}\rangle_{\Gamma_{\rm I}} = (\mathbf{f}_{\rm f},\mathbf{v})_{\Omega_{\rm f}}, \tag{14}$$

$$a_{\rm p}(\varphi_{\rm p},\psi)-\langle\mathbf{u}_{\rm f}\cdot\mathbf{n}_{\rm f},\psi\rangle_{\Gamma_{\rm I}} = (f_{\rm p},\psi)_{\Omega_{\rm p}}. \tag{15}$$

Here, the coupling is based on Neumann interface conditions for both the Stokes and the Darcy problem, and (14)–(15) will be therefore called a Neumann–Neumann coupled problem.

In order to describe better the different coupled formulations arising from the Stokes–Darcy problem, it is helpful to rewrite (14)–(15) in a more abstract form. Let $\mathcal{V}_{\rm f}=(V_{\rm f},Q_{\rm f})$ be the function space in which the solution (velocity and pressure) to the Stokes problem is sought, and let $\mathcal{V}_{\rm f}'$ denote its dual space. Similarly, let $Q_{\rm p}'$ denote the dual of $Q_{\rm p}$. Define the operators $\mathcal{S}:\mathcal{V}_{\rm f}\to\mathcal{V}_{\rm f}'$ and $\mathcal{D}:Q_{\rm p}\to Q_{\rm p}'$ such that

$$(\mathcal{D}\varphi,\psi) := a_{\rm p}(\varphi,\psi),$$

$$(\mathcal{S}s,t) := a_{\rm f}(\mathbf{u},\mathbf{v})+b_{\rm f}(\mathbf{v},p)-b_{\rm f}(\mathbf{u},q),$$

for all $s=(\mathbf{u},p),t=(\mathbf{v},q)\in\mathcal{V}_{\rm f}$, and $\varphi,\psi\in Q_{\rm p}$, and the coupling operator $\mathcal{C}:\mathcal{V}_{\rm f}\to Q_{\rm p}'$ by

$$(\mathcal{C}s,\psi) := \langle\mathbf{u}\cdot\mathbf{n}_{\rm f},\psi\rangle_{\Gamma_{\rm I}}.$$

Then, the Neumann–Neumann coupled problem (14)–(15) can be equivalently written as follows: Find $\varphi\in Q_{\rm p}$ and $s=(\mathbf{u},p)\in\mathcal{V}_{\rm f}$ such that

$$\begin{pmatrix}\mathcal{D} & -\mathcal{C}\\ g\mathcal{C}^\top & \mathcal{S}\end{pmatrix}\begin{pmatrix}\varphi\\ s\end{pmatrix} = \begin{pmatrix}\mathcal{F}_{\rm p}\\ \mathcal{F}_{\rm f}\end{pmatrix}. \tag{16}$$

The operator $\mathcal{C}^\top: Q_{\rm p}\to\mathcal{V}_{\rm f}'$ is the adjoint of $\mathcal{C}$, and the right-hand sides $\mathcal{F}_{\rm f}\in\mathcal{V}_{\rm f}'$ and $\mathcal{F}_{\rm p}\in Q_{\rm p}'$ are defined by

$$(\mathcal{F}_{\rm p},\psi) := (f_{\rm p},\psi)_{\Omega_{\rm p}}, \qquad (\mathcal{F}_{\rm f},t) := (\mathbf{f}_{\rm f},\mathbf{v})_{\Omega_{\rm f}},$$

for all $t=(\mathbf{v},q)\in\mathcal{V}_{\rm f}$ and all $\psi\in Q_{\rm p}$. An equivalent form of the Stokes–Darcy system can be obtained using Lagrange multipliers $\eta_{\rm f}$ and $\eta_{\rm p}$ on the interface $\Gamma_{\rm I}$. This approach formally decouples the Stokes and the Darcy subproblems by considering the system

$$\begin{pmatrix}\mathcal{D} & & & -\mathcal{E}_{\rm p}\\ \mathcal{R}_{\rm p} & -\mathcal{I} & & \\ & -\mathcal{E}_{\rm f} & \mathcal{S} & \\ & & \mathcal{R}_{\rm f} & -\mathcal{I}\end{pmatrix}\begin{pmatrix}\varphi\\ \eta_f\\ s\\ \eta_p\end{pmatrix} = \begin{pmatrix}\mathcal{F}_{\rm p}\\ 0\\ \mathcal{F}_{\rm f}\\ 0\end{pmatrix}, \tag{17}$$

where $\mathcal{I}$ is the identity operator,

$$(\mathcal{E}_{\rm f}\eta_{\rm f},t) = \langle\eta_{\rm f},\mathbf{v}\cdot\mathbf{n}_{\rm f}\rangle_{\Gamma_{\rm I}} \text{ and } (\mathcal{E}_{\rm p}\eta_{\rm p},\psi) = \langle\eta_{\rm p},\psi\rangle_{\Gamma_{\rm I}}$$

correspond to extension operators into the Stokes and Darcy domain, respectively, and

$$\mathcal{R}_{\rm p}:\psi\mapsto -g\psi|_{\Gamma_{\rm I}} \text{ and } \mathcal{R}_{\rm f}:t\mapsto\mathbf{v}|_{\Gamma_{\rm I}}\cdot\mathbf{n}_{\rm f},$$

are restriction operators from the two subdomains. Formulation (17) is equivalent to (16) since, by definition,

$$g\mathcal{C}^\top = -\mathcal{E}_{\rm f}\mathcal{R}_{\rm p} \text{ and } \mathcal{C}=\mathcal{E}_{\rm p}\mathcal{R}_{\rm f}.$$

2.3 Robin–Robin coupled formulation (D-RR)

Instead of the interface conditions (6) and (7), one can as well consider two linear combinations

$$\gamma_{\rm f}\mathbf{u}_{\rm f}\cdot\mathbf{n}_{\rm f}+\mathbf{n}_{\rm f}\cdot\mathbb{T}(\mathbf{u}_{\rm f},p_{\rm f})\cdot\mathbf{n}_{\rm f} = -\gamma_{\rm f}\mathbb{K}\nabla\varphi_{\rm p}\cdot\mathbf{n}_{\rm f}-g\varphi_{\rm p} \tag{18}$$

$$\gamma_{\rm p}\mathbb{K}\nabla\varphi_{\rm p}\cdot\mathbf{n}_{\rm f}-g\varphi_{\rm p} = -\gamma_{\rm p}\mathbf{u}_{\rm f}\cdot\mathbf{n}_{\rm f}+\mathbf{n}_{\rm f}\cdot\mathbb{T}(\mathbf{u}_{\rm f},p_{\rm f})\cdot\mathbf{n}_{\rm f} \tag{19}$$

on $\Gamma_{\rm I}$ where $\gamma_{\rm f}\geq 0$ and $\gamma_{\rm p}>0$ are constant. The conditions (18) and (19) correspond to Robin boundary conditions for the Stokes and Darcy subproblems, respectively. Inserting them into (12)–(13) leads to

$$a_{\rm f}(\mathbf{u}_{\rm f},\mathbf{v})+b_{\rm f}(\mathbf{v},p_{\rm f})-b_{\rm f}(\mathbf{u}_{\rm f},q)+\langle\gamma_{\rm f}\mathbf{u}_{\rm f}\cdot\mathbf{n}_{\rm f},\mathbf{v}\cdot\mathbf{n}_{\rm f}\rangle_{\Gamma_{\rm I}} +\langle g\varphi_{\rm p},\mathbf{v}\cdot\mathbf{n}\rangle_{\Gamma_{\rm I}}+\langle\gamma_{\rm f}\mathbb{K}\nabla\varphi_{\rm p}\cdot\mathbf{n}_{\rm f},\mathbf{v}\cdot\mathbf{n}_{\rm f}\rangle_{\Gamma_{\rm I}} = (\mathbf{f}_{\rm f},\mathbf{v})_{\Omega_{\rm f}}, \tag{20}$$

$$a_{\mathrm{p}}(\varphi_{\mathrm{p}},\psi)+\left\langle\frac{1}{\gamma_{\mathrm{p}}}g\varphi_{\mathrm{p}},\psi\right\rangle_{\Gamma_{\mathrm{I}}}-\langle\mathbf{u}_{\mathrm{f}}\cdot\mathbf{n}_{\mathrm{f}},\psi\rangle_{\Gamma_{\mathrm{I}}}+\left\langle\frac{1}{\gamma_{\mathrm{p}}}\mathbf{n}_{\mathrm{f}}\cdot\mathbb{T}(\mathbf{u}_{\mathrm{f}},p_{\mathrm{f}})\cdot\mathbf{n}_{\mathrm{f}},\psi\right\rangle_{\Gamma_{\mathrm{I}}}=(f_{\mathrm{p}},\psi)_{\Omega_{\mathrm{p}}},\tag{21}$$

which will be called the Robin–Robin coupled formulation. The restrictions $\gamma_{\mathrm{f}}\geq 0$ and $\gamma_{\mathrm{p}}>0$ guarantee positiveness of the bilinear forms. Introducing the operators $\mathcal{S}_{\Gamma_{\mathrm{I}}}$, $\mathcal{D}_{\Gamma_{\mathrm{I}}}$, $\mathcal{C}_{\mathrm{p}}$, and $\mathcal{C}_{\mathrm{f}}^{\top}$ defined by

$$\begin{aligned}\left(\mathcal{S}_{\Gamma_{\mathrm{I}}}s,t\right)&=\langle\mathbf{u}\cdot\mathbf{n}_{\mathrm{f}},\mathbf{v}\cdot\mathbf{n}_{\mathrm{f}}\rangle_{\Gamma_{\mathrm{I}}},\\ \left(\mathcal{D}_{\Gamma_{\mathrm{I}}}\varphi,\psi\right)&=\left\langle g\varphi_{\mathrm{p}},\psi\right\rangle_{\Gamma_{\mathrm{I}}},\\ \left(\mathcal{C}_{\mathrm{f}}^{\top}\varphi,t\right)&=\langle\mathbb{K}\nabla\varphi\cdot\mathbf{n}_{\mathrm{f}},\mathbf{v}\cdot\mathbf{n}_{\mathrm{f}}\rangle_{\Gamma_{\mathrm{I}}},\\ \left(\mathcal{C}_{\mathrm{p}}s,\psi\right)&=\langle\mathbf{n}_{\mathrm{f}}\cdot\mathbb{T}(\mathbf{u},p)\cdot\mathbf{n}_{\mathrm{f}},\psi\rangle_{\Gamma_{\mathrm{I}}},\end{aligned}$$

for all $s=(\mathbf{u},p)\in\mathcal{V}_{\mathrm{f}}$, $t=(\mathbf{v},q)\in\mathcal{V}_{\mathrm{f}}$, $\varphi,\psi\in Q_{\mathrm{p}}$, one can rewrite (20)–(21) as

$$\begin{aligned}\begin{pmatrix}\mathcal{F}_{\mathrm{p}}\\ \mathcal{F}_{\mathrm{f}}\end{pmatrix}&=\begin{pmatrix}\mathcal{D}_{\mathrm{rob}} & \mathcal{C}_{\mathrm{rob}}\\ \mathcal{C}_{\mathrm{rob}}^{\top} & \mathcal{S}_{\mathrm{rob}}\end{pmatrix}\begin{pmatrix}\varphi\\ s\end{pmatrix}\\ &:=\left(\begin{pmatrix}\mathcal{D} & -\mathcal{C}\\ g\mathcal{C}^{\top} & \mathcal{S}\end{pmatrix}+\begin{pmatrix}\gamma_{\mathrm{p}}^{-1} & \\ & \gamma_{\mathrm{f}}\end{pmatrix}\begin{pmatrix}\mathcal{D}_{\Gamma_{\mathrm{I}}} & \mathcal{C}_{\mathrm{p}}\\ \mathcal{C}_{\mathrm{f}}^{\top} & \mathcal{S}_{\Gamma_{\mathrm{I}}}\end{pmatrix}\right)\begin{pmatrix}\varphi\\ s\end{pmatrix}.\end{aligned}\tag{22}$$

Comparing with Eq. (16), one sees that the second term represents the additional operators in the Robin–Robin problem (20)–(21) in comparison with the Neumann–Neumann formulation (14)–(15).

Similarly to the Neumann–Neumann case, the introduction of the interface variables η_{f} and η_{p} leads to

$$\begin{pmatrix}\mathcal{D}_{\mathrm{rob}} & & & -\mathcal{E}_{\mathrm{p}}\\ \mathcal{R}_{\mathrm{p,rob}} & -\mathcal{I} & & \\ & -\mathcal{E}_{\mathrm{f}} & \mathcal{S}_{\mathrm{rob}} & \\ & & \mathcal{R}_{\mathrm{f,rob}} & -\mathcal{I}\end{pmatrix}\begin{pmatrix}\varphi\\ \eta_f\\ s\\ \eta_p\end{pmatrix}=\begin{pmatrix}\mathcal{F}_{\mathrm{p}}\\ 0\\ \mathcal{F}_{\mathrm{f}}\\ 0\end{pmatrix}.\tag{23}$$

Then, one defines for all $t=(\mathbf{v},q)\in\mathcal{V}_{\mathrm{f}}$ and all $\psi\in Q_{\mathrm{p}}$:

$$\begin{aligned}\mathcal{R}_{\mathrm{p,rob}}&:\psi\mapsto(-g\psi-\gamma_{\mathrm{f}}\mathbb{K}\nabla\psi\cdot\mathbf{n}_{\mathrm{f}})\big|_{\Gamma_{\mathrm{I}}},\\ \mathcal{R}_{\mathrm{f,rob}}&:t\mapsto\left(\mathbf{v}-\gamma_{\mathrm{p}}^{-1}\mathbf{n}_{\mathrm{f}}\cdot\mathbb{T}(\mathbf{v},q)\right)\big|_{\Gamma_{\mathrm{I}}}\cdot\mathbf{n}_{\mathrm{f}}.\end{aligned}$$

By construction, (23) is equivalent to Eq. (22), since

$$\mathcal{C}_{\mathrm{rob}}^{\top}=-\mathcal{E}_{\mathrm{f}}\mathcal{R}_{\mathrm{p,rob}}\quad\text{and}\quad\mathcal{C}_{\mathrm{rob}}=-\mathcal{E}_{\mathrm{p}}\mathcal{R}_{\mathrm{f,rob}}.$$

For standard finite element discretizations, it turns out that η_{f} and η_{p} are discontinuous functions; see Section 3.2. Therefore, this approach is called D-RR (discontinuous Robin–Robin).

2.4 A Robin–Robin formulation for the Neumann–Neumann problem (C-RR)

The Robin problems (20)–(21) require the computation of derivatives on Γ_{I}. In the context of finite element methods, this step usually reduces the approximation order, and it might result in a suboptimal accuracy. An alternative weak formulation, equivalent to the Neumann–Neumann formulation (16), but based on the solution of two Robin problems in the subdomains Ω_{f} and Ω_{p}, which overcomes this difficulty, was proposed in [9, 14]. Using the framework introduced above, this coupled formulation can be written in the form

$$\begin{pmatrix}\mathcal{D}+\gamma_{\mathrm{p}}^{-1}\mathcal{D}_{\Gamma_{\mathrm{I}}} & & & -\gamma_{\mathrm{p}}^{-1}\mathcal{E}_{\mathrm{p}}\\ -b\mathcal{R}_{\mathrm{p}} & -\mathcal{I} & & a\mathcal{I}\\ & -\mathcal{E}_{\mathrm{f}} & \mathcal{S}+\gamma_{\mathrm{f}}\mathcal{S}_{\Gamma_{\mathrm{I}}} & \\ & c\mathcal{I} & d\mathcal{R}_{\mathrm{f}} & -\mathcal{I}\end{pmatrix}\begin{pmatrix}\varphi\\ \eta_f\\ s\\ \eta_p\end{pmatrix}=\begin{pmatrix}\mathcal{F}_{\mathrm{p}}\\ 0\\ \mathcal{F}_{\mathrm{f}}\\ 0\end{pmatrix},\tag{24}$$

where the factors a, b, c, and d have to be determined in order to obtain a formulation equivalent to Eq. (16) (and to Eq. (17)). The choice of the form (24) is motivated by two reasons. Firstly, it prevents the subproblems to be coupled directly (first and third rows). An indirect coupling is enforced only through the interface functions η_{f} and η_{p}. Secondly, each interface function can be computed from the solution in a single subdomain (empty blocks in the second and fourth rows). The signs of the operators and the positions of γ_{f} and γ_{p} are chosen such that the resulting scheme coincides with the ones presented in [9, 14]. System (24) is equivalent to Eq. (16) if

$$\begin{cases}\eta_{\mathrm{p}}=\gamma_{\mathrm{p}}\mathbf{u}\cdot\mathbf{n}_{\mathrm{f}}+g\varphi & \text{in } \Lambda_{\mathrm{p}}',\\ \eta_{\mathrm{f}}=bg\varphi+a\eta_{\mathrm{p}} & \text{in } H^{1/2}(\Gamma_{\mathrm{I}}),\\ \eta_{\mathrm{f}}=\gamma_{\mathrm{f}}\mathbf{u}\cdot\mathbf{n}_{\mathrm{f}}-g\varphi & \text{in } \Lambda_{\mathrm{f}}',\\ \eta_{\mathrm{p}}=d\mathbf{u}\cdot\mathbf{n}_{\mathrm{f}}+c\eta_{\mathrm{f}} & \text{in } H^{1/2}(\Gamma_{\mathrm{I}}),\end{cases}\tag{25}$$

with the interface (trace) spaces

$$\begin{aligned}\Lambda_{\mathrm{f}}&:=\mathbf{V}_{\mathrm{f}}\cdot\mathbf{n}_{\mathrm{f}}\big|_{\Gamma_{\mathrm{I}}}=\left\{\mathbf{v}|_{\Gamma_{\mathrm{I}}}\cdot\mathbf{n}_{\mathrm{f}}\ :\ \mathbf{v}\in\mathbf{V}_{\mathrm{f}}\right\},\\ \Lambda_{\mathrm{p}}&:=Q_{\mathrm{p}}\big|_{\Gamma_{\mathrm{I}}}=\left\{\psi|_{\Gamma_{\mathrm{I}}}\ :\ \psi\in Q_{\mathrm{p}}\right\}.\end{aligned}$$

Remark 1 If the interface spaces Λ_{f} and Λ_{p} coincide, one can solve (25) for a, b, c, and d, obtaining

$$a=\frac{\gamma_{\mathrm{f}}}{\gamma_{\mathrm{p}}},\quad b=-1-a,\quad c=-1,\quad d=\gamma_{\mathrm{f}}+\gamma_{\mathrm{p}},$$

as done in [9].

Remark 2 The difference between the two Robin–Robin formulations is that (22) is derived starting from two Robin conditions in strong form, i.e., (18)–(19), while (24) is equivalent to two Robin problems obtained from the Neumann–Neumann form (14)–(15).

Remark 3 The formal differences of the methods are evident in comparison with (17), (23), and (24). Note that the Robin–Robin formulation (24) can only be written in an operator form using the Lagrange multipliers, as the interface variables η_f and η_p are coupled to each other; see Eq. (25).

It will be explained in Section 3.2 that standard finite element methods lead to continuous functions for η_f and η_p. Hence, this approach will be called C-RR (continuous Robin–Robin).

3 Robin–Robin subdomain iterative methods

In the literature, one finds the so-called sequential and parallel Robin–Robin subdomain iterative methods. This section starts by presenting the principal form of these algorithms. Then, the important issue of the definition of the boundary data at the interface will be considered. Finally, some details concerning the implementation of the algorithms will be presented, and possible stopping criteria of the iterative process will be discussed.

3.1 Sequential and parallel approaches

The considered sequential form of the iterative method was proposed and studied, e.g., in [12, 14].

Algorithm *S*. (Sequential or Gauss–Seidel-type iteration)

0. Given $\eta_p^0, \eta_f^0 \in L^2(\Gamma_I)$, $\gamma_f \geq 0$, $\gamma_p > 0$, $\theta \in (0, 1]$. Set $k = 0$.
1. Solve a Darcy problem with Robin data η_p^k yielding φ_p^{k+1}.
2. Update η_f^{k+1} using η_f^k, η_p^k, φ_p^{k+1}, and θ.
3. Solve a Stokes problem with Robin data η_f^{k+1} yielding $\left(\mathbf{u}_f^{k+1}, p_f^{k+1}\right)$.
4. Update η_p^{k+1} using η_p^k, η_f^{k+1}, $\mathbf{u}_f^{k+1}$, p_f^{k+1}, and θ.
5. If not converged, increase k by 1 and go to step 1.

A straightforward modification of Algorithm S into a version where the subproblems are solved in parallel was studied in [9].

Algorithm *P*. (Parallel or Jacobi-type iteration)

0. Given $\eta_p^0, \eta_f^0 \in L^2(\Gamma_I)$, $\gamma_f \geq 0$, $\gamma_p > 0$, $\theta \in (0, 1]$. Set $k = 0$.
1. Do in parallel:
   (a) Solve a Darcy problem with Robin data η_p^k yielding φ_p^{k+1}.
   (b) Solve a Stokes problem with Robin data η_f^k yielding $\left(\mathbf{u}_f^{k+1}, p_f^{k+1}\right)$.
2. Do in parallel:
   (a) Update η_f^{k+1} using η_f^k, η_p^k, φ_p^{k+1}, and θ.
   (b) Update η_p^{k+1} using η_p^k, η_f^k, $\mathbf{u}_f^{k+1}$, p_f^{k+1}, and θ.
3. If not converged, increase k by 1 and go to step 1.

The Robin problems to be solved in Algorithms S and P have the following form:

– Darcy: Find $\varphi_p^{k+1} \in Q_p$ such that for all $\psi \in Q_p$

$$a_p\left(\varphi_p^{k+1}, \psi\right) + \left\langle \frac{1}{\gamma_p} g \varphi_p^{k+1}, \psi \right\rangle_{\Gamma_I} = \left(f_p, \psi\right)_{\Omega_p} + \left\langle \frac{1}{\gamma_p} \eta_p^k, \psi \right\rangle_{\Gamma_I},$$

– Stokes: Find $\left(\mathbf{u}_f^{k+1}, p_f^{k+1}\right) \in V_f \times Q_f$ such that for all $(\mathbf{v}, q) \in V_f \times Q_f$

$$a_f\left(\mathbf{u}_f^{k+1}, \mathbf{v}\right) + b_f\left(\mathbf{v}, p_f^{k+1}\right) - b_f\left(\mathbf{u}_f^{k+1}, q\right) + \left\langle \gamma_f \mathbf{u}_f^{k+1} \cdot \mathbf{n}_f, \mathbf{v} \cdot \mathbf{n}_f \right\rangle_{\Gamma_I} = \left(\mathbf{f}_f, \mathbf{v}\right)_{\Omega_f} + \left\langle \eta_f^{\tilde{k}}, \mathbf{v} \cdot \mathbf{n}_f \right\rangle_{\Gamma_I},$$

where in Algorithm S it is $\tilde{k} = k + 1$ and in Algorithm P it is $\tilde{k} = k$.

The matrix-vector representations of the two Robin–Robin formulations (23) and (24) possess the structure

$$\begin{pmatrix} A_{11} & A_{12} \\ A_{21} & A_{22} \end{pmatrix} \begin{pmatrix} \begin{pmatrix} \varphi \\ \eta_f \end{pmatrix} \\ \begin{pmatrix} s \\ \eta_p \end{pmatrix} \end{pmatrix} = \begin{pmatrix} \begin{pmatrix} \mathcal{F}_p \\ 0 \end{pmatrix} \\ \begin{pmatrix} \mathcal{F}_f \\ 0 \end{pmatrix} \end{pmatrix}.$$

It can be seen that Algorithm S is a block Gauss–Seidel method (with a forward solve) for this system, whereas Algorithm P is a block Jacobi method; both methods are not damped. Both algorithms solve the subproblems involving the diagonal blocks A_{ii}, $i \in \{1, 2\}$, with one damped Gauss–Seidel step. Note that A_{ii}, $i \in \{1, 2\}$, are lower triangular two-by-two block matrices themselves, with one diagonal block typically much bigger than the other one. Hence, Algorithm P is, strictly speaking, a nested Jacobi and Gauss–Seidel algorithm.

With the introduced framework, a discussion of the expectations for the convergence of the subdomain iterative schemes with respect to small values of ν and K is possible. Considering the Jacobi and Gauss–Seidel method as fixed point iterations, then for the Neumann–Neumann coupling (16) (or (17)), the iteration matrices are given by

$$G_J := \begin{pmatrix} 0 & \mathcal{D}^{-1}\mathcal{C} \\ -\mathcal{S}^{-1} g \mathcal{C}^\top & 0 \end{pmatrix}, \quad G_{GS} := \begin{pmatrix} 0 & \mathcal{D}^{-1}\mathcal{C} \\ 0 & -\mathcal{S}^{-1} g \mathcal{C}^\top \mathcal{D}^{-1}\mathcal{C} \end{pmatrix}, \tag{26}$$

respectively. Let us use $\|G_J\|_\infty$ and $\|G_{GS}\|_\infty$ as a guidance for the asymptotic behavior of the iteration matrices as ν and K become small. A straightforward calculation of the inverse of $\mathcal{S}$ shows that $\|\mathcal{S}^{-1}\|_\infty = \mathcal{O}(\nu^{-1})$. It is clear that $\|\mathcal{D}^{-1}\|_\infty = \mathcal{O}(K^{-1})$. Since the matrices $\mathcal{C}$ and $g\mathcal{C}^\top$ do not depend on ν and K, one gets $\|G_J\|_\infty = (K^{-1} + \nu^{-1})$ and $\|G_{GS}\|_\infty = (K^{-1}(1+\nu^{-1}))$. Hence, the norms are large for small values of ν and K, and one cannot expect convergence in this situation.

For the D-RR method, the iteration matrices are of form (26) with the blocks given in Eq. (22). Inserting these blocks and using, e.g., $\mathcal{S}_{\text{rob}}^{-1} = \mathcal{O}((\nu+\gamma_f)^{-1})$, $\mathcal{C}_{\text{rob}} = \mathcal{O}(1+\gamma_p^{-1}(1+\nu))$ and so on, one obtains

$$\|G_{GS}\|_\infty = \mathcal{O}\left(\left(\frac{1-\nu K}{\nu+\gamma_f} + K\right) \times \left(\frac{1-K+\gamma_p^{-1}\nu}{K+\gamma_p^{-1}} + 1\right)\right). \quad (27)$$

The first factor becomes very small if γ_f is chosen to be very large. For the second factor, one obtains at best $\mathcal{O}(1)$, for instance, for $\gamma_p = \mathcal{O}(1)$ or γ_p small. Altogether, for small values of ν and K, one can expect a fast convergence if $0 < \gamma_p \leq \mathcal{O}(1)$ and $\gamma_f \gg \mathcal{O}(1)$.

For the C-RR method, the iteration matrices can be derived from (24) in straightforward, but somewhat lengthy, calculations, which will be omitted here for the sake of brevity. Both iteration matrices possess terms with $(\mathcal{S} + \gamma_f \mathcal{S}_{\Gamma_I})^{-1}$. Hence, for the iteration matrix not to depend on ν^{-1}, one has to choose $\gamma_f = \mathcal{O}(1)$ or larger. The smallness of other terms requires γ_f to be small, such that $\gamma_f = \mathcal{O}(1)$ seems to be a good compromise. Also for γ_p, one gets contradictory conditions if the smallness of the norm of the iteration matrices is required; hence, a good compromise is $\gamma_p = \mathcal{O}(1)$. These choices fit to the recommendations from [12, p. 398] on the size of the Robin parameters. The arguments used in this paper provide also the proposal to choose $\gamma_p < \gamma_f$. Altogether, for the C-RR updating strategy, there is no particular asymptotic choice of the Robin parameters which ensures the norm of the iteration matrix to be small for small ν and K.

3.2 The boundary conditions at the interface

A main issue of the algorithms is updating the Robin data η_f^{k+1} and η_p^{k+1}, steps 2 and 4 of Algorithm *S*, and step 2 of Algorithm *P*.

In [9, 12, 14], the following approach was considered, with $\theta = 1$,

$$\eta_f^{k+1} = (1-\theta)\eta_f^k + \theta\left(\frac{\gamma_f}{\gamma_p}\eta_p^k - \frac{\gamma_p+\gamma_f}{\gamma_p} g\varphi_p^{k+1}\right), \quad (28)$$

$$\eta_p^{k+1} = (1-\theta)\eta_p^k + \theta\left(-\eta_f^{\tilde{k}} + (\gamma_p+\gamma_f)\mathbf{u}_f^{k+1}\cdot\mathbf{n}_f\right). \quad (29)$$

This updating strategy is a damped version of applying the second and fourth lines in Eq. (25), i.e., it originates from the Robin–Robin formulation (24) for the Neumann–Neumann coupled problem (14)–(15). Using conforming finite element spaces, φ_p^{k+1} and $\mathbf{u}_f^{k+1}$ are continuous functions. Thus, if η_f^0 and η_p^0 are also continuous, then the updating strategy (28)–(29) gives also continuous Robin data at the interface. For this reason, it is denoted C-RR (continuous Robin–Robin) in this paper.

A different updating strategy consists in applying

$$\eta_f^{k+1} = (1-\theta)\eta_f^k + \theta\left(-g\varphi_p^{k+1} - \gamma_f \mathbb{K}\nabla\varphi_p^{k+1}\cdot\mathbf{n}_f\right), \quad (30)$$

$$\eta_p^{k+1} = (1-\theta)\eta_p^k + \theta\left(\gamma_p\mathbf{u}_f^{k+1}\cdot\mathbf{n}_f - \mathbf{n}_f\cdot\mathbb{T}(\mathbf{u}_f^{k+1}, p_f^{k+1})\cdot\mathbf{n}_f\right). \quad (31)$$

This strategy corresponds to the second and fourth rows of Eq. (23), together with a damping, i. e., it comes from a Robin–Robin formulation. Note that for continuous finite element spaces, $\nabla\varphi_p^{k+1}$ and $\mathbb{T}\left(\mathbf{u}_f^{k+1}, p_f^{k+1}\right)$ are in general discontinuous functions, such that Eqs. (30) and (31) lead to discontinuous Robin data η_f and η_p. Thus, this strategy is denoted D-RR (discontinuous Robin–Robin).

For $\theta = 1$, the updating strategy C-RR with Algorithm *S* is the Robin–Robin method that was analyzed in [14]. Together with Algorithm *P*, it was proposed and analyzed in [9]. Although both approaches are rather similar, the corresponding algorithms rely on completely different choices of the Robin parameters: $\gamma_f > \gamma_p$ for small ν and K in [14] and $\gamma_f < \gamma_p$ for unitary ν and K in [9]. In both cases, it was reported that the opposite choice would not lead to an efficient strategy. On the one hand, both papers [14] and [9] study different regimes of the coefficients of the Stokes–Darcy problem, but on the other hand, a dependence of the Robin parameters on these coefficients is not considered. Altogether, it remains still unclear how to choose the Robin–Robin parameters for given ν and K in general situations. We could find the use of the D-RR updating strategy only in [11], within Algorithm *S*.

3.3 Implementation aspects, stopping criteria

The matrices corresponding to the Darcy and Stokes problem do not change during the iterative processes in both Algorithms *S* and *P*. Therefore, one assembly prior to the iteration suffices and a factorization can be computed. Furthermore, the interface contribution $\left\langle \eta_f^{k+1}, \mathbf{v}\cdot\mathbf{n}\right\rangle_{\Gamma_I}$ (corresponding to $\mathcal{E}_f$ in Eqs. (23) and (24), which is added to the right-hand side of the Stokes system, is linear in η_f and can be computed by a matrix-vector multiplication. Similar ideas apply to the update of the right-hand side in the Darcy problem, i. e., to the operator $\mathcal{E}_p$, and to the restriction

operators $\mathcal{R}_\mathrm{p}$, $\mathcal{R}_\mathrm{f}$, $\mathcal{R}_{\mathrm{p,rob}}$, and $\mathcal{R}_{\mathrm{f,rob}}$ in Eqs. (23) and (24), respectively. Hence, no further assembling is needed during the iteration.

The simplified condition (9) is imposed weakly, penalizing the tangential component of the velocity on the interface by a Nitsche technique [15, 23], rather than enforcing it directly in the velocity function space.

Standard stopping criteria, e.g., the ones used in [12, 14], depend on the absolute or relative differences between successive iterates, computed on pressure or velocity solution vectors or on interface variables, i. e., based on terms of the form

$$\left\| s_h^{k+1} - s_h^k \right\|_{\ell^2} \quad \text{or} \quad \frac{\left\| s_h^{k+1} - s_h^k \right\|_{\ell^2}}{\left\| s_h^k \right\|_{\ell^2}},$$

where s_h^k stands for $\mathbf{u}_{\mathrm{f},h}^k$, $p_{\mathrm{f},h}^k$, $\varphi_{\mathrm{p},h}^k$, $\eta_{\mathrm{p},h}^k$, or $\eta_{\mathrm{f},h}^k$. In [12, 14], the relative increment of the discrete normal velocity on the interface $\mathbf{u}_{\mathrm{f},h} \cdot \mathbf{n}_\mathrm{f}|_{\Gamma_\mathrm{I}}$ was used. Another possibility consists in checking the accuracy of the coupling conditions (6) and (7). However, these stopping criteria only measure the progress of the iteration and not the quality of the solution, i. e., they are not able to detect whether the computed iterate is indeed close to the solution of the discrete problem or if the iteration sticks at an early stage. Therefore, we considered a further stopping criterion based on the residual of (the discrete versions of) Eq. (16) or (22), i.e.,

$$R_k := \left\| \begin{pmatrix} \mathcal{D}_h & \mathcal{C}_h \\ \mathcal{C}_h^\top & \mathcal{S}_h \end{pmatrix} \begin{pmatrix} \varphi_{\mathrm{p},h}^{k+1} \\ s_{\mathrm{f},h}^{k+1} \end{pmatrix} - \begin{pmatrix} \mathcal{F}_{\mathrm{f},h} \\ \mathcal{F}_{\mathrm{p},h} \end{pmatrix} \right\|_{\ell^2}.$$

If not stated otherwise, in the simulations presented in Section 4, the iterative procedure has been stopped when the following conditions were satisfied for a prescribed threshold eps > 0

$$\begin{cases} R_k < \mathrm{eps} \qquad \text{and} \\ \dfrac{\left\| \mathbf{u}_{\mathrm{f},h}^{k+1} - \mathbf{u}_{\mathrm{f},h}^k \right\|_{\ell^2}}{\left\| \mathbf{u}_{\mathrm{f},h}^k \right\|_{\ell^2}} + \dfrac{\left\| p_{\mathrm{f},h}^{k+1} - p_{\mathrm{f},h}^k \right\|_{\ell^2}}{\left\| p_{\mathrm{f},h}^k \right\|_{\ell^2}} \\ \quad + \dfrac{\left\| \varphi_{\mathrm{p},h}^{k+1} - \varphi_{\mathrm{p},h}^k \right\|_{\ell^2}}{\left\| \varphi_{\mathrm{p},h}^k \right\|_{\ell^2}} < \mathrm{eps}. \end{cases} \tag{32}$$

In the second condition, we omitted the denominator whenever it was smaller than one.

4 Computational results

The goal of the numerical studies consists in assessing Algorithms S and P in combination with the updating strategies C-RR and D-RR with respect to their efficiency. Since in all methods the numerical costs per iteration are very similar, the efficiency will be measured in terms of the number of iterations for reaching convergence. Because of our motivation to study applications in computational geosciences, the algorithms will be assessed especially for physical parameters which are relevant in this context.

For all numerical examples, the P_2/P_1 Taylor–Hood pair of finite element spaces was used for the velocity and pressure in the Stokes subdomain, while the P_2 element was used for the piezometric head. This choice of spaces is the same as, e.g., in [9, 12, 14]. The Robin–Robin updating strategies were applied with $\theta = 1$. All simulations were performed with the code MooNMD [18]. The linear systems of equations were solved with the sparse direct solver UMFPACK [10].

To verify the implementation, the solver was benchmarked considering a solution belonging to the finite element spaces. In these studies, the final errors for $\nu = 1$ and $\mathbb{K} = \mathbb{I}$ were of the order of the machine accuracy, but they increased with ν^{-1} and $\mathbb{K}^{-1}$. This observation reflects the fact that for small ν and $\mathbb{K}$, the condition numbers of the finite element linear systems increase.

As already mentioned above, a motivation for the present study is the unclear situation concerning the choice of the Robin parameters γ_f and γ_p. To address this question, we validated our implementation against two examples taken from [9, 12, 14], to reproduce the published results using the algorithms considered in the respective paper. In addition, all other algorithms were also assessed for these examples. Finally, an example related to a geoscientific application will be studied [7, 8]. For this example, a detailed investigation of the impact of the Robin parameters on the number of iterations will be presented.

4.1 Example 1

This example was used in [9] for illustrating the behavior of Algorithm P with the C-RR updating strategy for the viscosity $\nu = 1$ and the hydraulic conductivity $\mathbb{K} = \mathbb{I}$. Since the main goal of this example is the validation of our results against the results from [9], only the same coefficients will be considered.

Let $\Omega_\mathrm{p} = (0, \pi) \times (-1, 0)$, $\Omega_\mathrm{f} = (0, \pi) \times (0, 1)$, and $\Gamma_\mathrm{I} = (0, \pi) \times \{0\}$. The hydraulic conductivity has the form $\mathbb{K} = K\mathbb{I}$ and the solution of the coupled problem (1), (2), (5) is given by

$$\mathbf{u}_\mathrm{f}(x, y) = \begin{pmatrix} v'(y)\cos(x) \\ v(y)\sin(x) \end{pmatrix}, \quad p_\mathrm{f}(x, y) = 0,$$

$$\varphi_\mathrm{p}(x, y) = e^y \sin(x),$$

where

$$v(y) = -K - \frac{gy}{2\nu} + \left(-\frac{\alpha g}{4\nu^2} + \frac{K}{2} \right) y^2.$$

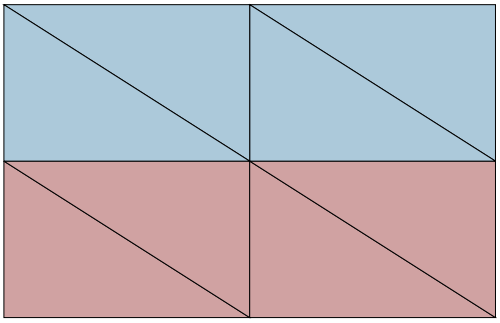

Fig. 1 Example 1: initial grid (level 0) with Ω_f in *blue* (*top*) and Ω_p in *red* (*bottom*)

On the outer boundaries, i. e., $\Gamma_{f,e} = \partial\Omega_f \setminus \Gamma_I$ and $\Gamma_{p,e} = \partial\Omega_p \setminus \Gamma_I$, essential boundary conditions were prescribed. This example considers the Beavers–Joseph–Saffman condition, i.e., the coupling conditions at the interface are given by Eqs. (6), (7), and (8). Numerical simulations were performed on meshes obtained by uniformly refining an initial coarse grid (level 0) consisting of eight triangles; see Fig. 1. Note that no information about the mesh is available in [9], such that our setup might be different in this respect. The initial iterate was always set to be zero. The iterative algorithm was stopped according to criterion (32) with a tolerance eps $= 10^{-10}$. The use of this stopping criterion is another difference to [9].

Figure 2 shows the evolution of the relative discrete errors of the iterates of the Stokes velocity for different choices of the Robin parameters. In all cases, the curves are in agreement with the results reported in [9, Fig. 6.1]. Details concerning the needed iterations are provided in Table 1. For the updating strategy D-RR, Algorithm *S* converged faster than Algorithm *P*. Moreover, for all methods, the number of iterations is independent of the level. As stated also in [9], one can see in Fig. 2 a very fast convergence if $\gamma_f < \gamma_p$, a slow convergence if $\gamma_f = \gamma_p$, and divergence in the case $\gamma_f > \gamma_p$. The speed of convergence depends essentially on the ratio γ_f/γ_p. In this example, the smallest number of iterations was needed for $\gamma_p = 1$. One can observe the same convergence behavior for the Stokes pressure and the piezometric head.

In summary, the results from [9] could be reproduced very well.

4.2 Example 2

This example was used in [12, 14] for assessing Algorithm *S* with the C-RR updating strategy for different values of the kinematic viscosity ν and the hydraulic conductivity K.

Let $\Omega_p = (0,1)^2$ and $\Omega_f = (0,1) \times (1,2)$, with the interface $\Gamma_I = \partial\Omega_p \cap \partial\Omega_f = (0,1) \times \{1\}$, the hydraulic conductivity of the form $\mathbb{K} = K\mathbb{I}$, and the solution given by

$$\begin{aligned} \mathbf{u}_f(x,y) &= \begin{pmatrix} y^2 - 2y + 1 \\ x^2 - x \end{pmatrix}, \\ p_f(x,y) &= 2\nu(x+y-1) + \frac{g}{3K}, \\ \varphi_p(x,y) &= \frac{1}{K}\left(x(1-x)(y-1) + \frac{y^3}{3} - y^2 + y\right) \\ &\quad + \frac{2\nu}{g}x. \end{aligned} \tag{33}$$

The Dirichlet boundary conditions were imposed on $\partial\Omega_f \setminus \Gamma_I$ and on the bottom boundary $(0,1) \times \{0\}$. On the remaining parts, Neumann boundary conditions were prescribed. Furthermore, (6) and (7) together with the simplified Beavers–Joseph–Saffman condition (9) were considered. We used unstructured grids with 98 (mesh 1), 470 (mesh 2), 1,914 (mesh 3), and 8,216 (mesh 4) cells with a total of 406 (mesh 1), 1,690 (mesh 2), 6,553 (mesh 3), and 27,402 (mesh 4) degrees of freedom. The initial iterate was always chosen to be zero.

Using values for the parameters ν and K relevant for geoscientific applications, which are typically very small, the pressure and the piezometric head in Eq. (33) consist of two parts, a very small contribution scaled with ν and a very large part due to the scaling with K^{-1}. This second part leads to values of p_f and φ_p which are unrealistic in applications. In this respect, this example has some deficiencies.

To reproduce the results from [12, 14], we first used as stopping criterion only

$$\frac{\|\mathbf{u}_f^{k+1} - \mathbf{u}_f^k\|}{\|\mathbf{u}_f^k\|} < 10^{-6}, \tag{34}$$

similarly as it has been applied in [12, 14], where the relative increment of the discrete normal velocity on the interface and a somewhat smaller tolerance were used. Note that $\mathbf{u}_f$ is the only part of the solution that does not scale with K^{-1}. Because of the large condition number of the linear system of equations for small ν and K, which was already mentioned above, one generally has to relax the tolerances of stopping criteria in this case compared with the case $\nu = 1$, $K = 1$.

Table 2 reports the results with Robin parameters $\gamma_p = 1$, $\gamma_f = \gamma_p/3$, which was the most efficient choice in Example 1, in combination with the stopping criterion (34). Clearly, all algorithms failed for those parameters in the case of small ν and small K.

Indeed, following [12, 14] and the considerations at the end of Section 3.1, one would expect efficient simulations for a different choice of the Robin parameters, for instance, for $\gamma_p = 0.1$, $\gamma_f = 3\gamma_p$. In this case, one obtains the

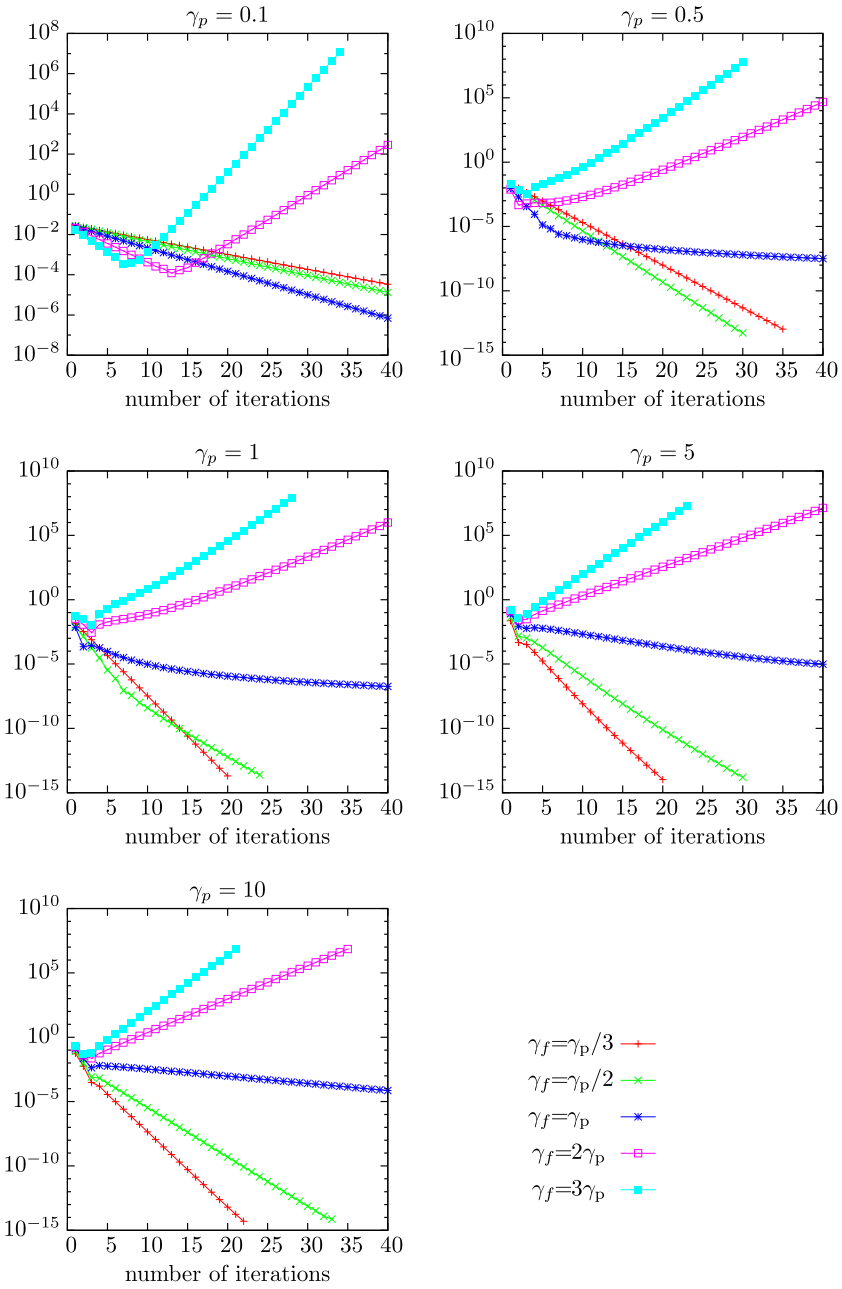

Fig. 2 Example 1: relative discrete errors $\frac{\left\|\mathbf{u}_{f,h}^{k+1}-\mathbf{u}_{f,h}\right\|_{\ell^2}}{\|\mathbf{u}_{f,h}\|_{\ell^2}}$ of Algorithm S with $\nu = 1$ and $K = 1$, different values of γ_p and γ_f, refinement level 4

results presented in Table 3. One can see that the algorithms with the updating strategy D-RR converged for all choices of physical parameters. We observed a similar behavior of the algorithms with the D-RR updating strategy also for $\gamma_f = 3\gamma_p$ with $\gamma_p \in \{1, 10, 50, 100, 200\}$. The results are similar to those reported in [12, 14] for the updating strategy C-RR. In our simulations, however, the C-RR updating strategy was less successful for many studied choices of the

Table 1 Example 1: number of iterations for $\gamma_p = 1$ and $\gamma_f = \gamma_p/3$

Updating strategy	Algorithm	Level			
		1	2	3	4
C-RR	Algorithm P	19	19	19	20
C-RR	Algorithm S	19	19	19	20
D-RR	Algorithm P	34	36	36	36
D-RR	Algorithm S	19	19	19	20

Table 2 Example 2: number of iterations for $\gamma_p = 1$ and $\gamma_f = \gamma_p/3$, stopping criterion (34)

Updating strategy	Algorithm	ν	K	Mesh 1	Mesh 2	Mesh 3	Mesh 4
C-RR	Algorithm P	1	1	7	7	7	7
		10	10^{-1}	25	25	25	25
		10^{-2}	10^{-2}	–	–	–	–
	Algorithm S	1	1	7	7	7	7
		10	10^{-1}	11	11	11	11
		10^{-2}	10^{-2}	–	–	–	–
D-RR	Algorithm P	1	1	9	9	11	11
		10	10^{-1}	18	20	20	20
		10^{-2}	10^{-2}	+++	+++	+++	+++
	Algorithm S	1	1	5	6	7	7
		10	10^{-1}	10	11	11	11
		10^{-2}	10^{-2}	–	–	–	–
Neumann–Neumann	Both	10^{-3}	10^{-2}	–	–	–	–
		10^{-4}	10^{-3}	–	–	–	–
C-RR, D-RR		10^{-6}	10^{-4}	–	–	–	–
		10^{-6}	10^{-7}	–	–	–	–

"+++" means did not converge within 100 iterations and "–" means diverged

Robin parameters, which is in agreement with the considerations at the end of Section 3.1, and we could not reproduce the results from [12, 14]. Consulting the Ph.D. thesis [11], one gets the impression that in [12, 14], the C-RR updating strategy is presented and analyzed, but the numerical studies in these papers were performed with the D-RR updating strategy.

In Table 3, one can see that Algorithm *P* was (for the D-RR updating strategy) more efficient than Algorithm *S* for very small values of the physical coefficients. For both algorithms, the number of iterations is independent of the mesh.

Next, the convergence properties of the algorithms using the harder stopping criterion (32), also with eps $= 10^{-6}$, were investigated. One can observe in Fig. 3 that for $\gamma_p = 0.1$ and $\gamma_f = 3\gamma_p$ (we obtained similar results for $\gamma_p \in \{\frac{1}{30}, \frac{1}{3}, 1\}$), even if criterion (34) is satisfied, the residual of the complete coupled problem is far from being small. Figure 3 shows also that the relative changes of the pressure and the piezometric head are still large. For further

Table 3 Example 2: number of iterations for $\gamma_p = 0.1$ and $\gamma_f = 0.3$, stopping criterion (34)

Type	Algorithm	ν	K	Mesh 1	Mesh 2	Mesh 3	Mesh 4
C-RR	Algorithm P	10^{-4}	10^{-3}	–	–	–	–
		10^{-6}	10^{-4}	–	–	–	–
		10^{-6}	10^{-7}	–	–	–	–
	Algorithm S	10^{-4}	10^{-3}	207	51	27	21
		10^{-6}	10^{-4}	274	12	12	12
		10^{-6}	10^{-7}	12	12	12	12
D-RR	Algorithm P	10^{-4}	10^{-3}	15	15	17	17
		10^{-6}	10^{-4}	7	9	9	9
		10^{-6}	10^{-7}	7	9	9	9
	Algorithm S	10^{-4}	10^{-3}	11	11	11	11
		10^{-6}	10^{-4}	12	12	12	12
		10^{-6}	10^{-7}	12	12	12	12

"–" means diverged

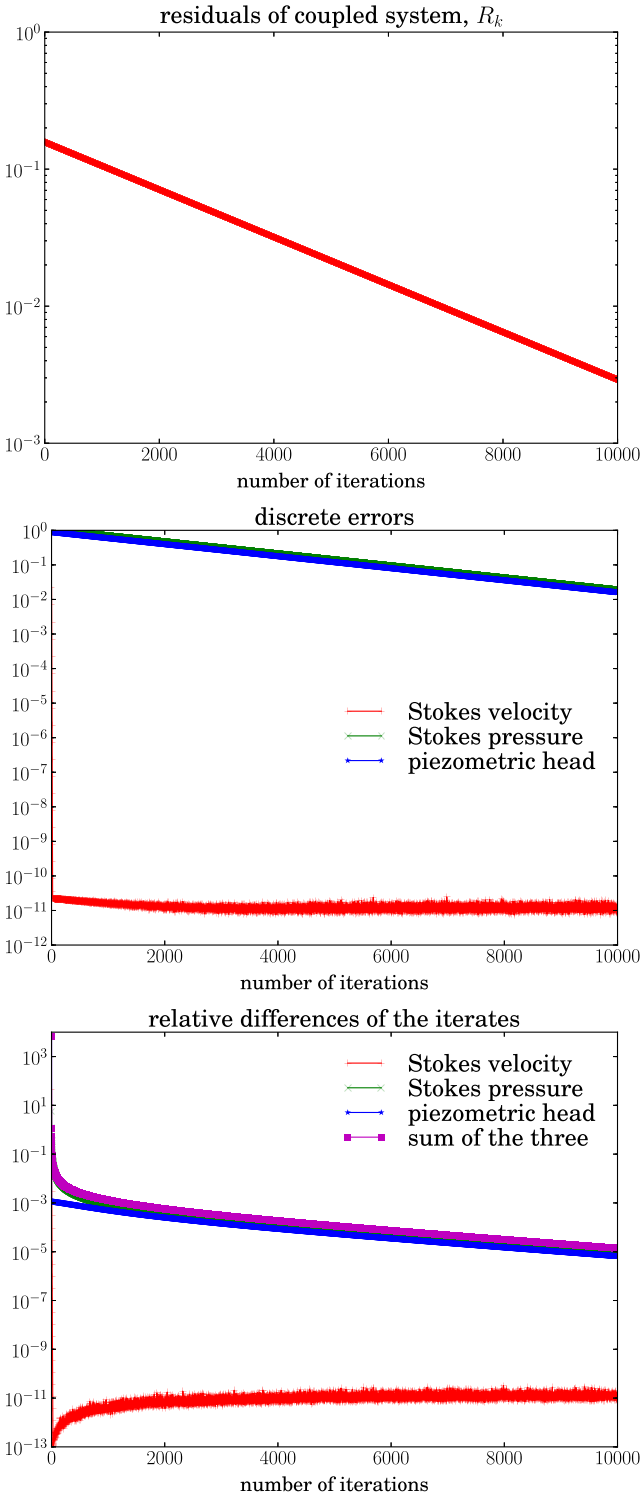

Fig. 3 Example 2: evolution of the residual, discrete errors, and relative differences for Algorithm *S*, mesh 4, D-RR updating strategy with $\gamma_p = 0.1$, $\gamma_f = 3\gamma_p$, $\nu = 10^{-4}$, and $K = 10^{-3}$

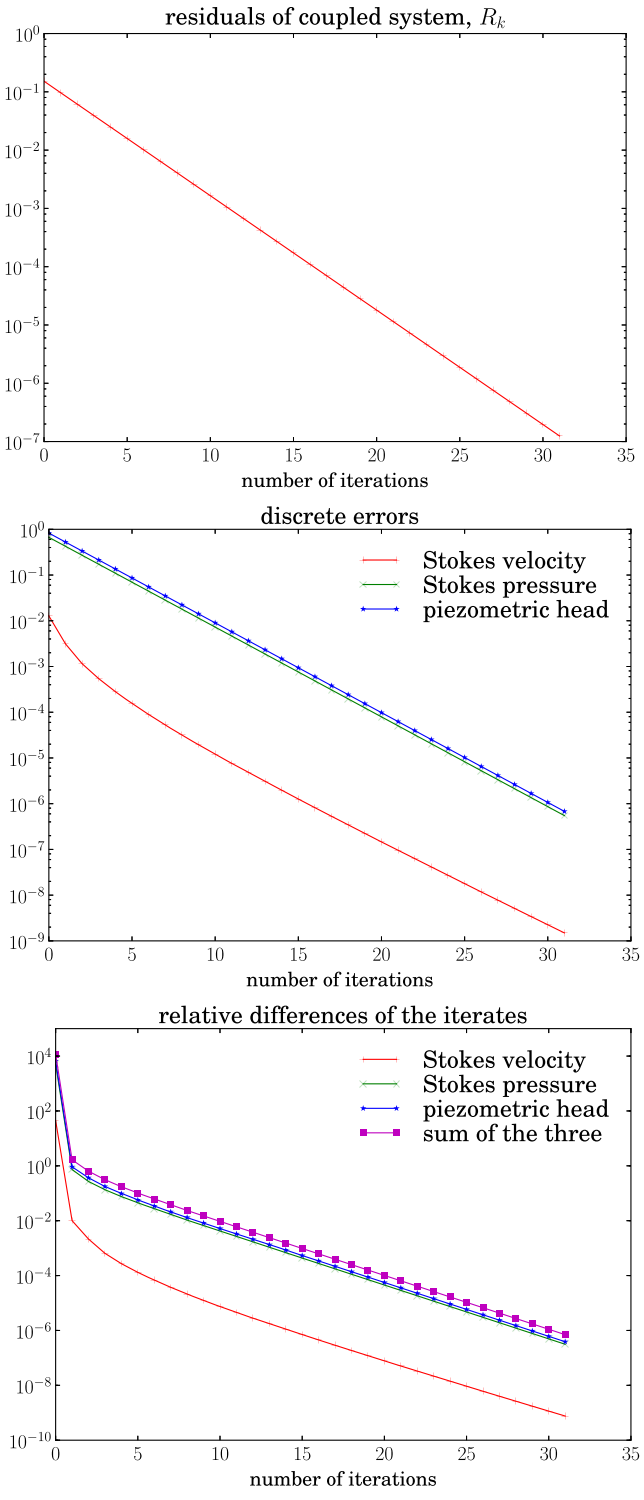

Fig. 4 Example 2: evolution of the residual, discrete errors, and relative differences for Algorithm *S*, mesh 4, D-RR updating strategy with $\gamma_p = 100$, $\gamma_f = 3\gamma_p$, $\nu = 10^{-4}$, and $K = 10^{-3}$

comparisons, we computed the solution of the monolithic discrete Stokes–Darcy problem by applying a direct solver to the coupled finite element problem (an approach which is not feasible in many applications). Then, one can see that the iterates for the pressure and the piezometric head still differ considerably from the discrete solution. These observations confirm that the stopping criterion (34) is not sufficient to assess the properties of the

Table 4 Example 2: number of iterations for $\gamma_p = 100$ and $\gamma_f = 300$, stopping criterion (32)

Type	Algorithm	ν	K	Mesh 1	Mesh 2	Mesh 3	Mesh 4
C-RR	Algorithm P	10^{-4}	10^{-3}	–	–	–	–
		10^{-6}	10^{-4}	–	–	–	–
		10^{-6}	10^{-7}	–	–	–	–
	Algorithm S	10^{-4}	10^{-3}	–	–	–	–
		10^{-6}	10^{-4}	432	422	413	–
		10^{-6}	10^{-7}	+++	+++	+++	+++
D-RR	Algorithm P	10^{-4}	10^{-3}	76	74	72	71
		10^{-6}	10^{-4}	841	823	805	787
		10^{-6}	10^{-7}	+++	+++	+++	+++
	Algorithm S	10^{-4}	10^{-3}	32	32	32	32
		10^{-6}	10^{-4}	326	316	307	298
		10^{-6}	10^{-7}	+++	+++	+++	+++

"+++" means did not converge within 1,000 iterations, "–" means diverged

iterative algorithms, and the number of iterations given in Table 3 might provide a wrong impression of their efficiency.

Further numerical studies revealed that a considerable speedup of the algorithms with the D-RR updating strategy could be achieved by increasing the Robin parameters, thereby keeping the relation $\gamma_f = 3\gamma_p$; see Fig. 4 and Table 4. Similar results were obtained for $\gamma_p \in \{50, 200\}$. We think that the slow convergence in the case $K = 10^{-7}$ is due to the unrealistic large values for the pressure and the hydraulic head. One can see in Table 4 that Algorithm *S* performed better than Algorithm *P*. The number of iterations is independent of the mesh.

In summary, despite the shortcomings of the used example, it was clarified that for the case of small viscosity and small hydraulic conductivity, the use of the D-RR updating strategy and the choice $\gamma_f > \gamma_p$ of the Robin parameters are important to obtain an efficient subdomain iteration.

4.3 Example 3: water flow over a porous river bed

As a final example, a model of a unidirectional steady water flow over a porous bed is considered, separated by a nonstraight interface. In the context of computational geosciences, this model has been proposed for the study of the hydrodynamic interactions between the water flow and the underlying river bed [7, 8].

In order to simulate the water flow over two triangular dunes, consider a rectangular domain

$$\Omega = [0, 2L] \times [0, H_f + H_p],$$

where H_f and H_p denote the heights of the water flow domain and the porous river bed at $x \in \{0, L, 2L\}$. The interface, representing the dune, is composed of two triangles, whose highest points are located at $x \in \{l_D, L + l_D\}$, while the maximum height of the dunes, with respect to the entrance porous bed, is denoted by h_D; see Fig. 5.

The boundary conditions and the values of the physical parameters have been chosen as in the numerical simulations presented in [7, 8]. In particular, the lower boundary is considered impermeable (no flux boundary condition), while no-slip conditions are imposed at the upper boundary (note that the arrows in Fig. 6 are unscaled). For inlet and outlet boundaries, the following inhomogeneous periodic

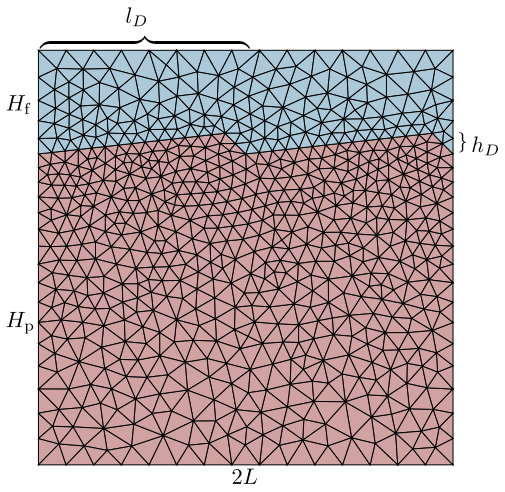

Fig. 5 Example 3: computational domain, triangulated with mesh 1

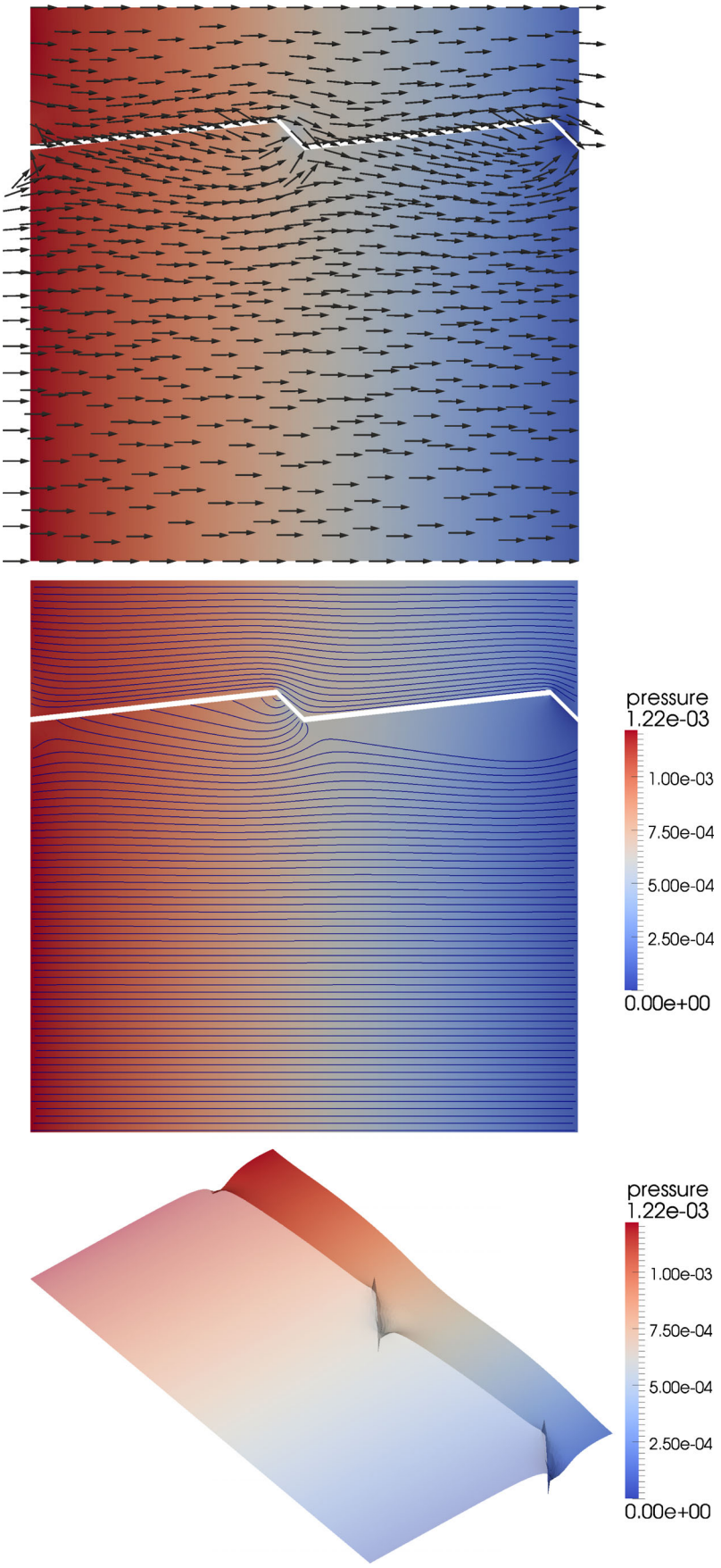

Fig. 6 Example 3: numerical solution for $v = 10^{-6}$ and $K = 10^{-7}$, velocity field $\mathbf{u}_f$ and $\nabla\varphi_p$ (unscaled arrows, *top*), velocity streamlines (*middle*), pressure elevation (*bottom*); *color* is always p_f and φ_p

Table 5 Example 3: information concerning the meshes

Mesh	Interface edges	Mesh cells		Degrees of freedom	
		Stokes	Darcy	Stokes	Darcy
1	32	277	1,009	1,392	2,098
2	68	1,285	4,513	6,093	9,196
3	138	5,234	18,322	24,181	36,987

boundary conditions for the Stokes and the Darcy problem have been imposed:

$$\begin{aligned} \mathbf{u}_{\text{inlet}} &= \mathbf{u}_{\text{outlet}}, \\ \mathbb{T}(\mathbf{u}_{\text{inlet}}, p_{\text{inlet}}) \cdot \mathbf{n}_{\text{f}} &= -\mathbb{T}(\mathbf{u}_{\text{outlet}}, p_{\text{outlet}}) \cdot \mathbf{n}_{\text{f}} + p_0 \mathbf{n}_{\text{f}}, \\ \varphi_{\text{inlet}} &= \varphi_{\text{outlet}} + p_0, \\ -\mathbb{K}\nabla\varphi_{\text{inlet}} \cdot \mathbf{n}_{\text{f}} &= \mathbb{K}\nabla\varphi_{\text{outlet}} \cdot \mathbf{n}_{\text{f}}\,. \end{aligned}$$

Note that the pressure is unique only up to an additive constant in this example. We fixed this constant by forcing one pressure node to be zero. Furthermore, the simulation parameters are

$$L = 1,\ H_{\text{f}} = 0.5,\ H_{\text{p}} = 1.5,\ l_D = 0.9,\ h_D = 0.1,$$
$$p_0 = 10^{-3},\ \mathbf{f}_{\text{f}} = 0,\ f_{\text{p}} = 0.$$

Figure 6 depicts the numerical solution for $\nu = 10^{-6}$ and $K = 10^{-7}$. The prescribed pressure drop p_0 induces a flow from left to right, which partially penetrates the porous bed due to the inclination of the interface. However, the impact of the water flow onto the porous media (and vice versa) remains local, i. e., the flow remains unperturbed and unidirectional away from the interface. Note the pressure drop arising behind the dunes, which locally causes a flow in the opposite direction underneath the dunes.

Three different unstructured meshes were considered in the numerical simulations; see Fig. 5 for an example and Table 5 for detailed information. Based on the results obtained in Example 2, we decided to employ the updating strategy D-RR in combination with Algorithm *S*. The obtained number of iterations for all combinations of $K \in \{10^{-7}, 10^{-6}, 10^{-5}, 10^{-4}, 10^{-3}\}$ and $\nu \in \{10^{-6}, 10^{-5}, 10^{-4}\}$ are presented in Fig. 7. Several values of γ_{p} and ratios $\gamma_{\text{f}}/\gamma_{\text{p}}$ were considered. It can be seen that for very small values of ν and K, the number of iterations is independent of the mesh size. For fixed γ_{p}, the larger the ratio $\gamma_{\text{f}}/\gamma_{\text{p}}$ is, the smaller the number of iterations becomes. One can observe two situations where the convergence of the method is slow. In the first situation, where γ_{p} is small (left-hand side pictures of Fig. 7), the condition $\gamma_{\text{f}} \geq \mathcal{O}(1)$ is not satisfied. The other situation can be observed in the pictures on the right-hand side of Fig. 7, where γ_{p} is large. From Eq. (27), one gets that for K and ν small, the norm of the iteration matrix scales like $\mathcal{O}(K(1+1/(K+\gamma_{\text{p}}^{-1})))$. As long as γ_{p} is small, this term is $\mathcal{O}(K)$, whereas it becomes $\mathcal{O}(1)$ if γ_{p} approaches K^{-1}. In summary, if ν and K are small, then for a fast convergence, a large ratio $\gamma_{\text{f}}/\gamma_{\text{p}}$ is of advantage, which is much larger than proposed so far in the literature. From Fig. 7, one can deduce that a suitable choice which works for all considered values of ν and K is $\gamma_{\text{p}} = \mathcal{O}(1)$.

One should be aware on the impact of the values of the Robin parameters on the computational results of the D-RR updating strategy. These parameters determine the approximation quality of the interface conditions (6) and (7), relative to each other, by the numerical solution. In Fig. 8, the results on mesh 3 are presented; for the two other meshes, qualitatively the same results were obtained. One can observe that the ratio of the error in the flux condition $\|\mathbf{u}_{\text{f}} \cdot \mathbf{n}_{\text{f}} + \mathbb{K}\nabla\varphi_{\text{p}} \cdot \mathbf{n}_{\text{f}}\|_{L^2(\Gamma_{\text{I}})}$ and the normal stress condition $\|\mathbf{n}_{\text{f}} \cdot \mathbb{T}(\mathbf{u}_{\text{f}}, p_{\text{f}}) \cdot \mathbf{n}_{\text{f}} + g\varphi_{\text{p}}\|_{L^2(\Gamma_{\text{I}})}$ depends on $\gamma_{\text{f}}/\gamma_{\text{p}}$. For fixed γ_{p}, the larger $\gamma_{\text{f}}/\gamma_{\text{p}}$ is, the smaller is the flux error compared with the normal stress error. In addition, the ratio of the errors depends also on the actual choice of γ_{p}. For fixed $\gamma_{\text{f}}/\gamma_{\text{p}}$, one finds that the larger γ_{p}, the smaller the flux error becomes compared with the normal stress error. Choosing both γ_{f} and γ_{p} large favors (6) over (7), which can be already deduced from (18)–(19). Thus, if for a considered application the accurate approximation of one of the interface conditions (6) or (7) is more important than the other, one has to take this aspect into account for the choice of the Robin parameters. Note that the incorporation of the residual R_k into the stopping criterion (32) guarantees a certain accuracy of the solution with respect to both interface conditions.

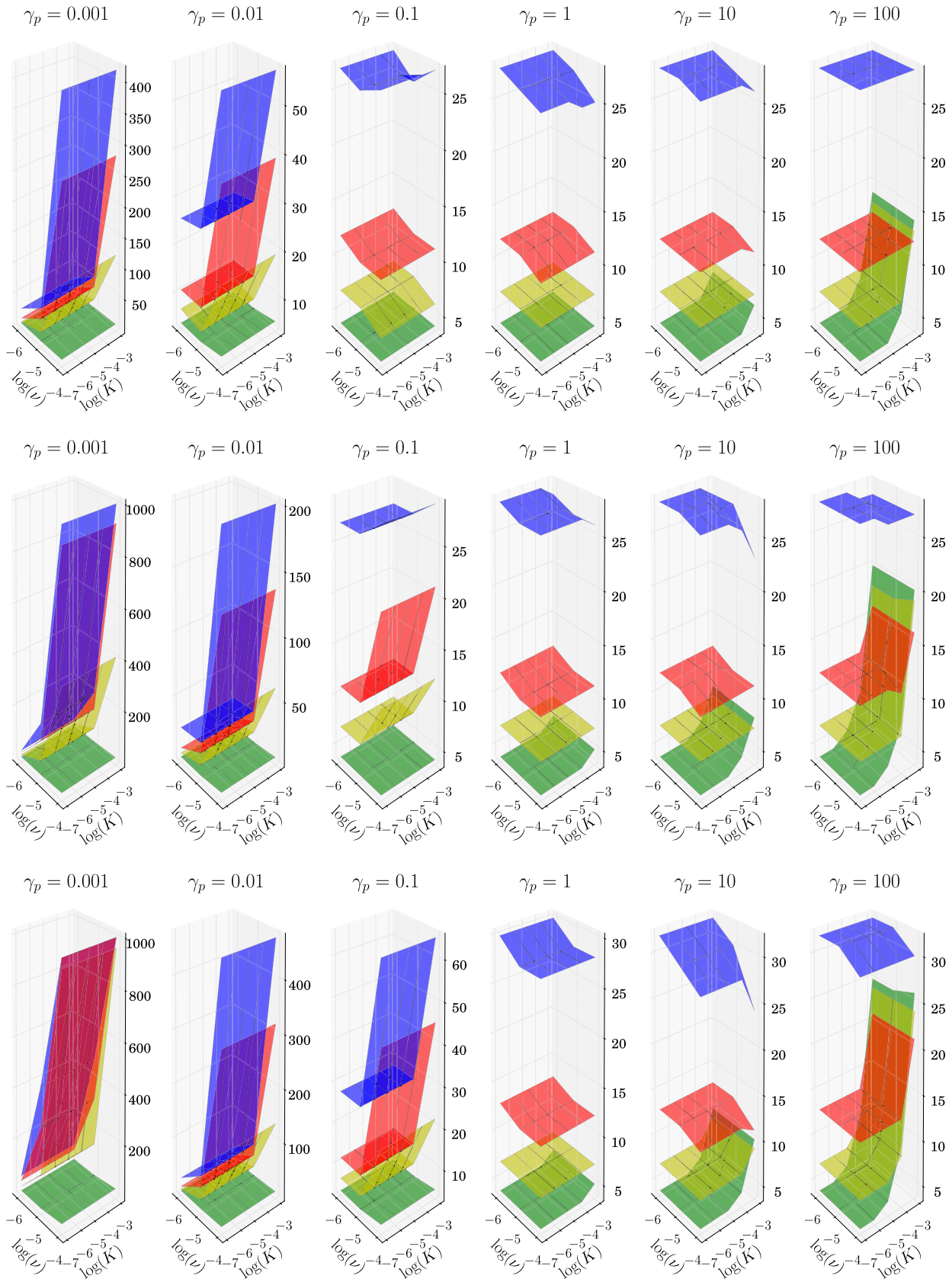

Fig. 7 Example 3: number of iterations on mesh 1, 2, 3 (*top to bottom*), Algorithm *S* with D-RR updating strategy: $\gamma_f = 1.5\gamma_p$ (*blue*), $\gamma_f = 3\gamma_p$ (*red*), $\gamma_f = 10\gamma_p$ (*yellow*), $\gamma_f = 1{,}000\gamma_p$ (*green*). Note the different scaling of the z-axes; 1,000 iterations means did not converge

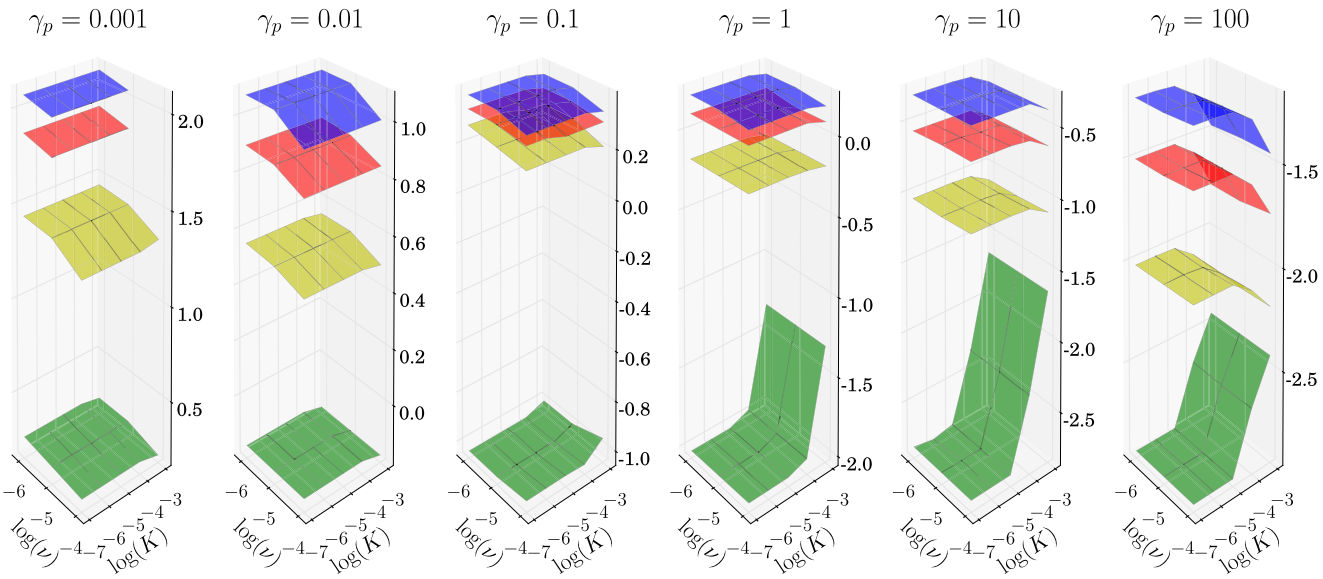

Fig. 8 Example 3: $\log\left(\|\mathbf{u}_f \cdot \mathbf{n}_f + \mathbb{K}\nabla\varphi_p \cdot \mathbf{n}_f\|_{L^2(\Gamma_I)} / \|\mathbf{n}_f \cdot \mathbb{T}(\mathbf{u}_f, p_f) \cdot \mathbf{n}_f + g\varphi_p\|_{L^2(\Gamma_I)}\right)$ for mesh 3, Algorithm *S* with D-RR updating strategy: $\gamma_f = 1.5\gamma_p$ (*blue*), $\gamma_f = 3\gamma_p$ (*red*), $\gamma_f = 10\gamma_p$ (*yellow*), $\gamma_f = 1{,}000\gamma_p$ (*green*)

5 Summary and outlook

This paper reviewed some classical iterative subdomain methods for solving the Stokes–Darcy problem which use Robin boundary conditions at the interface. In particular, it was clarified that there are different updating strategies for the Robin boundary conditions. For coefficients in the Stokes–Darcy problem that are relevant for applications from geosciences, the use of the updating strategy D-RR, in combination with an appropriate choice of the Robin parameters, turned out to be crucial for designing an efficient numerical method. A detailed numerical study, together with some considerations on the asymptotic of the norm of the iteration matrices for small viscosity and hydraulic conductivity, gave new insight into appropriate choices for the Robin parameters. In particular, it was shown that efficient methods can be obtained for ratios γ_f/γ_p which are much larger than proposed so far in the literature. Finally, it was observed that the serial update of the interface conditions, Algorithm *S*, needed often less iterations than the parallel update, Algorithm *P*.

Altogether, the main goal of our studies was accomplished: the identification of an efficient iterative subdomain method for the Stokes–Darcy problem with coefficients that are relevant in geosciences.

Further research includes studies of classical iterative subdomain methods for the Navier–Stokes–Darcy problem and a detailed investigation for the dual formulation of the Darcy problem, focusing on relevant situations for geoscientific applications. Another goal is the derivation of algorithms which embed the subdomain iteration with Robin interface conditions into Krylov subspace methods for a system defined on the interface.

Acknowledgements The research of Ulrich Wilbrandt has been supported by the "Helmholtz graduate research school GeoSim."

References

1. Angot, P.: On the well-posed coupling between free fluid and porous viscous flows. Appl. Math. Lett. **24**, 803–810 (2011)
2. Arbogast, T., Brunson, D.S.: A computational method for approximating a Darcy-Stokes system governing a vuggy porous medium. Comput. Geosci. **11**, 207–218 (2007)
3. Badia, S., Codina, R.: Unified stabilized finite element formulations for the Stokes and the Darcy problems. SIAM J. Numer. Anal. **47**, 1971–2000 (2009)
4. Burman, E., Hansbo, P.: A unified stabilized method for Stokes' and Darcy's equations. J. Comput. Appl. Math. **198**(1), 35–51 (2007)
5. Cao, Y., Gunzburger, M., Hu, X., Hua, F., Wang, X., Zhao, W.: Finite element approximations for Stokes-Darcy flow with Beavers-Joseph interface conditions. SIAM J. Numer. Anal. **47**(6), 4239–4256 (2010)
6. Cao, Y., Gunzburger, M., Hua, F., Wang, X.: Coupled Stokes-Darcy model with Beavers-Joseph interface boundary condition. Commun. Math. Sci. **8**(1), 1–25 (2010)
7. Cardenas, M., Wilson, J.: Dunes, turbulent eddies, and interfacial exchange with permeable sediments. Water Resour. Res. **43**(08), 412 (2007)
8. Cardenas, M., Wilson, J.: Hydrodynamics of coupled flow above and below a sediment–water interface with triangular bedforms. Adv. Water Resour. **30**, 301–313 (2007)
9. Chen, W., Gunzburger, M., Hua, F., Wang, X.: A parallel Robin-Robin domain decomposition method for the Stokes-Darcy system. SIAM. J. Numer. Anal. **49**(3), 1064–1084 (2011)

10. Davis, T.A.: Algorithm 832: UMFPACK V4.3—an unsymmetric-pattern multifrontal method. ACM Trans. Math. Softw. **30**(2), 196–199 (2004)
11. Discacciati, M.: Domain decomposition methods for the coupling of surface and groundwater flows. PhD thesis, École Polytechnique Fédérale de Lausanne (2004)
12. Discacciati, M., Quarteroni, A.: Navier-Stokes/Darcy coupling: modeling, analysis, and numerical approximation. Rev. Mat. Complut. **22**(2), 315–426 (2009)
13. Discacciati, M., Quarteroni, A., Miglio, E.: Mathematical and numerical models for coupling surface and groundwater flows. Appl. Numer. Math. **43**, 57–74 (2002)
14. Discacciati, M., Quarteroni, A., Valli, A.: Robin-Robin domain decomposition methods for the Stokes-Darcy coupling. SIAM J. Numer. Anal. **45**(3), 1246–1268 (2007). (electronic)
15. Freund, J., Stenberg, R.: On weakly imposed boundary conditions for second order problems. In: Proceedings of the 9th International Conference Finite Elements in Fluids (1995)
16. Gatica, G.N., Oyarzua, R., Sayas, F.J.: Analysis of fully-mixed finite element methods for the Stokes-Darcy coupled problem. Math. Comput. **80**, 1911–1948 (2011)
17. Jaeger, W., Mikelic, A.: On the interface boundary condition of Beavers, Joseph and Saffman. SIAM J. Appl. Math. **60**(4), 1111–1127 (2000)
18. John, V., Matthies, G.: MooNMD—a program package based on mapped finite element methods. Comput. Vis. Sci. **6**(2–3), 163–169 (2004)
19. Jones, I.: Low Reynolds number flow past a porous spherical shell. Math. Proc. Cambridge Philos. Soc **73**, 231–238 (1973)
20. Layton, W., Schieweck, F., Yotov, I.: Coupling fluid flow with porous media flow. SIAM J. Numer. Anal. **40**, 2195–2218 (2003)
21. Levy, T., Sanchez-Palencia, E.: On the boundary condition for fluid flow in porous media. Int. J. Eng. Sci. **13**, 923–940 (1975)
22. Mardal, K., Tai, X.C., Winther, R.: A robust finite element method for Darcy-Stokes flow. SIAM J. Numer. Anal. **40**, 1605–1631 (2002)
23. Nitsche, J.: Über ein Variationsprinzip zur Lösung von Dirichlet-Problemen bei Verwendung von Teilräumen, die keinen Randbedingungen unterworfen sind. Abh. Math. Sem. Univ. Hamburg **36**, 9–15 (1971). Collection of articles dedicated to Lothar Collatz on his 60th birthday
24. Riviére, B., Yotov, I.: Locally conservative coupling of Stokes and Darcy flows. SIAM J. Numer. Anal. **42**, 1955–1977 (2005)
25. Saffman, P.: On the boundary condition at the interface of a porous medium. Stud. Appl. Math. **50**, 93–101 (1971)
26. Urquiza, J., N'Dri, D., Garon, A., Delfour, M.: Coupling Stokes and Darcy equations. Appl. Numer. Mathe **58**(5), 525–538 (2008)
27. Xie, X., Xu, J., Xue, G.: Uniformly-stable finite element methods for Darcy-Stokes-Brinkman models. J. Comput. Math. **26**, 437–455 (2008)
28. Zunino, P., D'Angelo, C.: Robust numerical approximation of coupled Stokes' and Darcy's flows applied to vascular hemodynamics and biochemical transport. ESAIM Math. Model. Numer. Anal. **45**(3), 447–476 (2011)